

Mathematical models of topologically protected transport in twisted bilayer graphene

Guillaume Bal ^{*} Paul Cazeaux [†] Daniel Massatt [‡] Solomon Quinn [§]

June 14, 2022

Abstract

Twisted bilayer graphene gives rise to large moiré patterns that form a triangular network upon mechanical relaxation. If gating is included, each triangular region has gapped electronic Dirac points that behave as bulk topological insulators with topological indices depending on valley index and the type of stacking. Since each triangle has two oppositely charged valleys, they remain topologically trivial.

In this work, we address several questions related to the edge currents of this system by analysis and computation of continuum PDE models. Firstly, we derive the bulk invariants corresponding to a single valley, and then apply a bulk-interface correspondence to quantify asymmetric transport along the interface. Secondly, we introduce a valley-coupled continuum model to show how valleys are approximately decoupled in the presence of small perturbations using a multiscale expansion, and how valleys couple for larger defects. Thirdly, we present a method to prove for a large class of continuum (pseudo-)differential models that a quantized asymmetric current is preserved through a junction such as a triangular network vertex.

We support all of these arguments with numerical simulations using spectral methods to compute relevant currents and wavepacket propagation.

1 Introduction

Twisted bilayer graphene (tBLG) is widely studied for its unique mechanical and electronic properties including the magic angle superconductivity [10, 24]. Upon gating, it acts as host of a network of topological interface channels, which can be seen experimentally and theoretically [27, 26, 12, 1]. tBLG is constructed by taking two periodic 2D sheets of graphene and stacking them with a relative twist, typically small. The atoms relax to minimize energy, forming large triangular regions of the energetically favorable AB and BA Bernal stacking [28, 11, 13]. It is relevant to note this asymmetric transport under gating is a separate phenomena from magic angle superconductivity. Indeed, the asymmetric transport phenomena only requires sufficiently small twist angles and vertical gating, i.e. by inducing a potential difference between the two layers, while superconductivity can only occur precisely at the magic twist angles. In this section, we make use of Figure 1 for discussion of the geometry.

The interior of one of these triangles can be considered as approximately an infinite periodic material. We note that in this work we will consider only continuum models and not lattice models, but for understanding

^{*}Departments of Statistics and Mathematics and CCAM, University of Chicago, Chicago, IL 60637; guillaumebal@uchicago.edu

[†]Department of Mathematics, Virginia Tech, Blacksburg, VA 24060; cazeaux@vt.edu

[‡]Department of Mathematics, Louisiana State University, Baton Rouge, LA 70803; dmassatt@lsu.edu

[§]Department of Statistics and CCAM, University of Chicago, Chicago, IL 60637; solomonquinn@uchicago.edu

of the purpose and origins of the continuum models in this work, it is useful to see the lattice model origins. If \mathcal{L} is the lattice matrix corresponding to the periodicity of the material, we define the reciprocal lattice unit cell as $\Gamma^* := 2\pi\mathcal{L}^{-T}[0, 1]^2$. Consider periodic Hamiltonian H describing the infinitely extended bulk corresponding to one of the triangular regions. Its spectra, which in turn describes electronic properties, can be described by the Bloch states satisfying

$$H(\xi)\psi^{(j)}(\xi) = E^{(j)}(\xi)\psi^{(j)}(\xi), \quad \xi \in \Gamma^* \quad (1.1)$$

where $H(\xi) = e^{-i\xi \cdot r} H e^{i\xi \cdot r}$. This expression is understood as operator composition. We assume $E^{(1)}(\xi) \leq E^{(2)}(\xi) \leq \dots$ are the ordered eigenvalues (or energies). Gating opens a band gap at $E = 0$, meaning all $E^{(j)}(\xi)$ are bounded away from 0. A topological integer index can be associated with the operator H by the formula

$$I[H] := \sum_{j \geq n} \frac{i}{2\pi} \int_{\Gamma^*} d(\psi^{(j)}, d\psi^{(j)}). \quad (1.2)$$

Here n is the smallest index such that $E^n(\xi) > 0$ for all $\xi \in \Gamma^*$. $I[H]$ can be computed by expanding only around the Dirac points $K, K' \in \Gamma^*$ as they possess the topological information. A local in momentum Hamiltonian $H(\xi)$ can be constructed for each of these valleys through a 4×4 model as follows:

$$H(\xi) := \begin{pmatrix} \Omega I + \xi_1 \sigma_1 + \eta \xi_2 \sigma_2 & \lambda U^* \\ \lambda U & -\Omega I + \xi_1 \sigma_1 + \eta \xi_2 \sigma_2 \end{pmatrix}. \quad (1.3)$$

Here $\eta = 1$ for valley K and $\eta = -1$ for valley K' , $\Omega \in \mathbb{R}$ measures the electrostatic potential difference between the two layers due to vertical gating, and $U \in \{A, A^*\}$ is the interlayer coupling term, where $A = \begin{pmatrix} 0 & 1 \\ 0 & 0 \end{pmatrix}$ [22]: A^* and A correspond to whether the triangle has AB or BA stacking geometry respectively.

This Hamiltonian has been rescaled to ensure Fermi velocity is 1 and unitless, i.e. there is no prefactor in front of the Dirac term $\xi_1 \sigma_1 + \xi_2 \sigma_2$. A standard result in topological insulators is the bulk-interface correspondence [8, 17], which states that if two topological materials are glued together at an interface, then there is quantized edge transport given by the difference of the topological index on either side of the interface; See [4, 5, 25] for the derivation of the correspondence for differential models. In bilayer graphene the K and K' valleys contribute opposite signed topological charge, so gated bilayer graphene is technically trivial. However, it is understood that the two valleys in many settings decouple, with each valley Hamiltonian having possibly nontrivial topology, which is the basis of *valleytronics* [30, 31].

In this work, we address gated tBLG via numerics and analysis of continuum models built to address three different questions corresponding to the two regions highlighted in Figure 1. For the first question addressed in Section 2, we use the 4×4 single-valley bulk model, compute its topological invariant, and then using the corresponding interface model apply the bulk-interface correspondence at an edge between two triangles (region 1). In particular, we make use of the bulk-difference invariant [5] between AB and BA stacked graphene for a single valley to find a quantized current of ± 2 . In Section 3, we focus on analyzing the separation of the K and K' valley at the interface (region 1). Since the 4×4 bilayer graphene model is only accurate near the valleys, we study valley coupling with a toy 2×2 model that exhibits two conical Dirac points. To model defects, we consider a two-scale model to introduce fast small fluctuations, and show the valley coupling is weak in this regime. We use numerics and scattering theory to further show that as the defects are tuned to couple the valleys, then valley separation breaks and quantized edge current is lost. In Section 4, we define a conductivity that quantifies the asymmetric transport through a junction (e.g. region 2). Following pseudodifferential calculus arguments from [25], we derive an analytic formula for this junction conductivity and show that the latter is immune to perturbations. This allows for explicit evaluations of the conductivity for both the 4×4 bilayer graphene and 2×2 Dirac models. Finally in Section

5, we include numerical verification of results from the preceding sections using spectral methods to properly capture the Dirac operator. Direct computation of traces is used to compute currents either isolated to the edge (Region 1) and currents through a junction (Region 2), and wavepacket propagation is used to illustrate the connection between the two regions by evolving a state localized on an edge through a network junction.

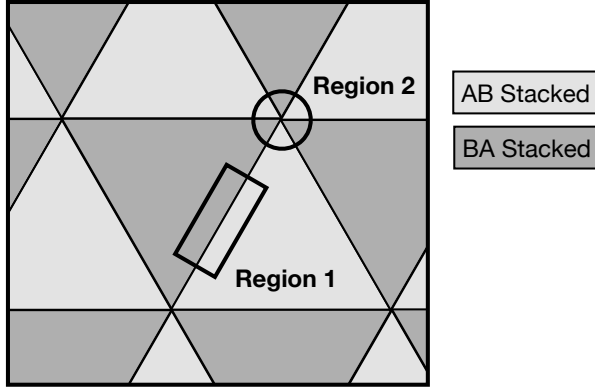


Figure 1: Triangular domains form in mechanically relaxed tBLG. We highlight two regions of interest for our analysis. Region 1 corresponds to an edge, where a standard bulk-interface correspondence will be studied as well as a continuum valley coupling model. Region 2 is at a junction, where we will analyze current conservation.

2 Gated tBLG model

In this section, we analyze region 1 from Figure 1 and use the bulk-interface correspondence to show quantized asymmetric transport for a single valley. To begin, we consider the bulk Hamiltonian in (1.3) described by the continuum model

$$H = \begin{pmatrix} \Omega I + D \cdot \sigma^{(\eta)} & \lambda U^* \\ \lambda U & -\Omega I + D \cdot \sigma^{(\eta)} \end{pmatrix}.$$

Here $\sigma^{(\eta)} := (\sigma_1, \eta\sigma_2)$, and $\xi \cdot \sigma^{(\eta)} := \xi_1\sigma_1 + \eta\xi_2\sigma_2$ where we recall $\eta \in \pm 1$ is the valley index. We will sometimes denote $\sigma^{(1)}$ by σ . This operator in two-dimensional physical variables is an unbounded operator on $L^2(\mathbb{R}^2; \mathbb{C}^4)$. The operator in the Fourier variables is given as in (1.3) for each $\xi \in \mathbb{R}^2$ by the 4×4 matrix:

$$H(\xi) = \begin{pmatrix} \Omega + \xi \cdot \sigma^{(\eta)} & \lambda U^* \\ \lambda U & -\Omega + \xi \cdot \sigma^{(\eta)} \end{pmatrix}.$$

These models are defined on a plane \mathbb{R}^2 , and hence are not defined over a compact manifold. To construct topological invariants, we introduce as in [5] the bulk-difference invariant describing the difference between AB and BA stacked graphene, the two bulks enclosing an interface. The two bulk Hamiltonians are given by

$$H_+(\xi) = \begin{pmatrix} \Omega I + \xi \cdot \sigma^{(\eta)} & \lambda A^* \\ \lambda A & -\Omega I + \xi \cdot \sigma^{(\eta)} \end{pmatrix},$$

$$H_-(\xi) = \begin{pmatrix} \Omega I + \xi \cdot \sigma^{(\eta)} & \lambda A \\ \lambda A^* & -\Omega I + \xi \cdot \sigma^{(\eta)} \end{pmatrix}.$$

The spectral projectors denoted $\xi \rightarrow |\psi_{\pm}^{(j)}(\xi)\rangle\langle\psi_{\pm}^{(j)}(\xi)|$ can be glued together continuously along the circle at infinity as $|\xi| \rightarrow \infty$ (see Figure 2), which allows the system to be parametrized over the compact sphere. More explicitly, we define the integral of the Berry curvature [8]

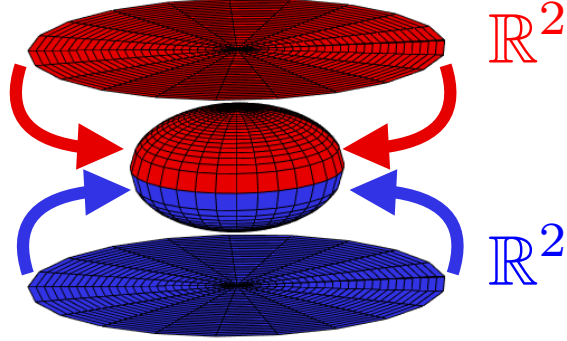


Figure 2: $(\pm, \xi) \rightarrow |\psi_{\pm}^{(j)}(\xi)\rangle\langle\psi_{\pm}^{(j)}(\xi)|$ is mapped to the sphere by mapping each plane \pm onto a hemisphere while preserving continuity along the ‘circle at infinity’.

$$W_{\pm} := \frac{i}{2\pi} \sum_{j=3}^4 \int_{\mathbb{R}^2} d(\psi_{\pm}^{(j)}, d\psi_{\pm}^{(j)}). \quad (2.1)$$

Note that the sum in (2.1) is over the two indices j corresponding to eigenvalues of H_{\pm} above the spectral gap at 0. The bulk-difference invariant, seen as an integral in ξ over the sphere as described above, is defined as

$$W = W_- - W_+. \quad (2.2)$$

Each term W_{\pm} separately is not naturally defined as an invariant and in fact takes values in $\pm 1/2$ when H is the Dirac operator [5]. The gluing procedure presented in Fig. 2 allows one to define a continuous function over a sphere, whose integral W may indeed be interpreted as an invariant guaranteed to take integral values; see [5] for more details. Heuristically, this result also shows that it is easier to define a difference of phases of insulators, which is all we need to characterize asymmetric transport between insulators, rather than absolute phases, which are ill-defined for Dirac-type operators.

We will compare this bulk invariant to an edge current, which describes asymmetric transport along an interface separating the bulk phases and is defined next. Firstly, we introduce an edge model by making the bulk above into a continuum model with an interface:

$$H_e := \begin{pmatrix} \Omega I + D \cdot \sigma^{(\eta)} & \lambda U^*(y) \\ \lambda U(y) & -\Omega I + D \cdot \sigma^{(\eta)} \end{pmatrix} \quad (2.3)$$

with $U(y) = m(y)A + (1 - m(y))A^*$ and $D = (D_x, D_y) = \frac{1}{i}(\partial_x, \partial_y)$. We choose m such that for large y we obtain BA stacking, while for large negative y we obtain AB stacking. In order to do this, we define the switch function space $\mathfrak{S}(c_1, c_2; y_1, y_2)$ defined such that $f \in \mathfrak{S}(c_1, c_2; y_1, y_2)$ is a smooth function satisfying

$$f(y) = \begin{cases} c_1, & y \leq y_1 \\ c_2, & y \geq y_2 \end{cases}.$$

We assume $m \in \mathfrak{S}(0, 1; -y_0, y_0)$ for some $y_0 > 0$. We define an edge state capturing energy function $\varphi \in \mathfrak{S}(0, 1; -E_0, E_0)$ where $E_0 > 0$ is chosen to be smaller than the bulk band gap. We have not yet shown there is a bulk band gap, but prove this below in Theorem 2.1. We note that φ' is supported in the gap, and thus $\varphi'(H_e)$ captures edge state spectra only. Finally we define a spatial projection $P \in \mathfrak{S}(0, 1; -x_0, x_0)$ for some $x_0 > 0$. The rate of propagation of current through the edge of P is given by [2, 5, 16, 23]

$$\sigma_I := \text{Tr } i[H_e, P]\varphi'(H_e). \quad (2.4)$$

The main objective of this section is to show that $2\pi\sigma_I = -W = 2\eta$. The first equality is a bulk-interface correspondence, which has been derived in a variety of contexts [2, 5, 16, 23, 25], and in particular in [5, 25] for the operators of interest here. The advantage of such a correspondence is that the explicit computation of W is often simpler than that of σ_I . We will obtain the former by adapting results derived in [7].

The Fourier transform of H_e can be taken along the interface, obtaining the Hamiltonian

$$H_e(\xi_1) = \begin{pmatrix} \Omega I + \xi_1 \sigma_1 + \eta D_y \sigma_2 & \lambda U^*(y) \\ \lambda U(y) & -\Omega I + \xi_1 \sigma_1 + \eta D_y \sigma_2 \end{pmatrix}. \quad (2.5)$$

In Kronecker product notation, this yields

$$H_e(\xi_1) = \Omega \sigma_3 \otimes I_2 + I_2 \otimes (\xi_1 \sigma_1 + \eta D_y \sigma_2) + \frac{1}{2}(\sigma_1 \otimes \sigma_1 + m(y) \sigma_2 \otimes \sigma_2). \quad (2.6)$$

In Figure 4, we plot the bulk band structure and superimpose the eigenvalues within the bulk band gap of a periodized version of $H_e(\xi_1)$, where we only include eigenvalues weighted towards one interface. This is necessary as the periodization creates a second domain wall with oppositely directed edge states. We then see that there are two right-ward propagating states, as expected (two curves crossing the bulk band gap with positive group velocity $\partial E / \partial \xi$). We note that the symmetry in the edge states $E(\xi_1) = -E(-\xi_1)$ comes from the following symmetry operation. Let $K = \sigma_2 \otimes \sigma_1$. Then

$$K^{-1} H_e(\xi_1) K = -H_e(-\xi_1).$$

To prove $-W = 2\eta$, the first step will be verifying there is indeed a bulk gap, which turns out to have a ring shape. We then use this to calculate the bulk-difference invariant W . This is done by continuously tuning the interlayer coupling λ towards 0. We can then study the Berry curvature of the ring through an effective 2×2 model over $S^1 \times \mathbb{R}$ as done in [7]. See Figure 3 to see concentration of Berry curvature on the ring and the corresponding band structure. Combining the above yields our main result:

Theorem 2.1. *The bulk system H has a band gap for all $\lambda \neq 0$. Further,*

$$W_{\pm} = \pm \eta \text{sign}(\Omega). \quad (2.7)$$

The bulk-interface correspondence then gives us

$$2\pi\sigma_I = -W = 2\eta \text{sign}(\Omega). \quad (2.8)$$

Proof. The proof of this result is postponed to Appendix A. \square

We note that we assumed an ordering to the AB and BA stacking. If we switch the order, we would swap the sign of W , and hence σ_I . Hence each edge has an edge current dependent on the order of the AB-BA regions and also the valley index of interest (see Figure 5).

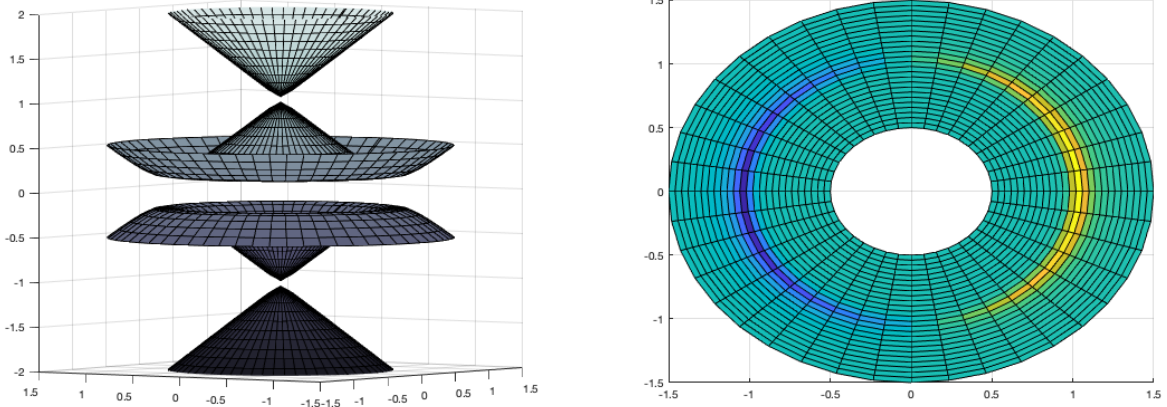


Figure 3: Here we plot the eigenvalues of $H(\xi)$, i.e. the band structure on the left. On the right, we plot the Berry curvature, or the integrand of (2.1). Here we set $\lambda = 0.2$ and $\Omega = 1$. As expected, curvature concentrates on the line $|\xi| = 1$. We include the annulus with radii $1/2$ and $3/2$ as well, which is used in Theorem 2.1.

We note that the structure of the Hamiltonians H and H_e are identical to the so called *2-replica model* static Hamiltonian used to approximate the dynamics of the circularly polarized laser-driven graphene system, which is a Floquet Topological Insulator [7, 29]. The reason these two very different physical systems share a common Hamiltonian is that in both situations the bulk systems are described as a coupling between Dirac cones shifted relative to each other in energy. The overlapping cones' intersection forms a ring, and the coupling between these Dirac cones hybridizes the bands to form ring-shaped band gaps. We remark that we expect bulk multilayer stacked graphene with all layers either AB stacked or BA stacked form the larger *replica* systems corresponding to a collection of uniformly shifted Dirac cones. Here the number of replicas or shifted Dirac cones corresponds to the number of sheets, while in the Floquet setting the number corresponded to the number of included time Fourier frequencies. In keeping with the Floquet terminology, we also refer to our Hamiltonians H and H_e as a *2-replica model* as it corresponds to two shifted Dirac cones.

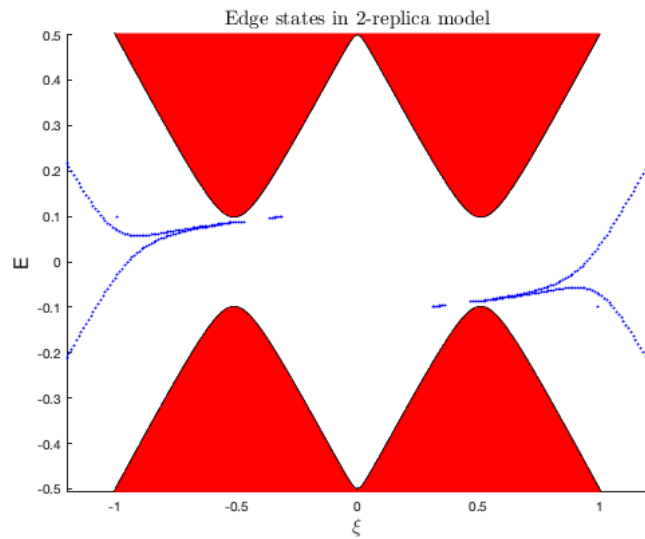


Figure 4: Bulk band structure (filled) is plotted along with calculated edge state eigenvalues (points) of a periodized $H_e(\xi_1)$. In particular, the plotted interface eigenvalues are the nearest two eigenvalues to $E = 0$.

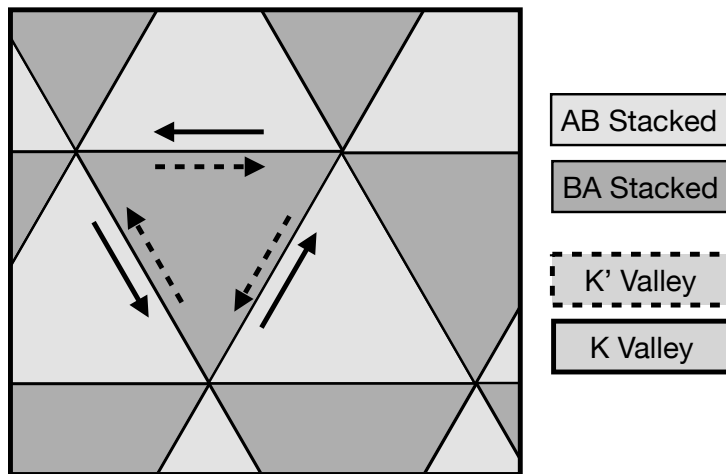


Figure 5: K and K' valley current directions are shown for each edge. Note that the currents per valley are always moving in opposite directions.

3 Valley Coupling

As we saw from the previous section, both valley Hamiltonians are topologically non-trivial. However, if valley coupling is allowed, then the total asymmetric current summed over the two valleys vanishes making the total system topologically trivial.

In section 3.1, we introduce a simplified differential operator that captures the two-valley physics, and construct one-dimensional and two-dimensional effective valley-coupling models using a multiscale expansion. In section 3.2, we then define a valley conductivity object. In section 3.3, we use numerics to calculate currents demonstrating what regime of defects yield good valley separation, and when does valley decoupling fail. In section 3.4 we use scattering theory to explain the numeric results from section 3.3.

3.1 Valley coupling models

To model a two-valley system and inter-valley coupling, consider first the bulk Hamiltonian without mass

$$H_b = \Phi(D_x)\sigma_1 + D_y\sigma_2.$$

Here Φ is some function with two zeros corresponding to two Dirac points. In frequency space, we denote the wavenumber pair $(\xi, \zeta) \in \mathbb{R}^2$. We have changed the notation from section 2 as now we wish to emphasize the direction along the edge ξ . We have

$$H_b(\xi, \zeta) = \Phi(\xi)\sigma_1 + \zeta\sigma_2,$$

which admits band structure. We will assume for simplicity of presentation throughout this section that the Dirac points are located at frequencies $(\xi, \zeta) = (\pm 1, 0)$. For example, see Figure 6 for $\Phi(\xi) = |\xi| - 1$.

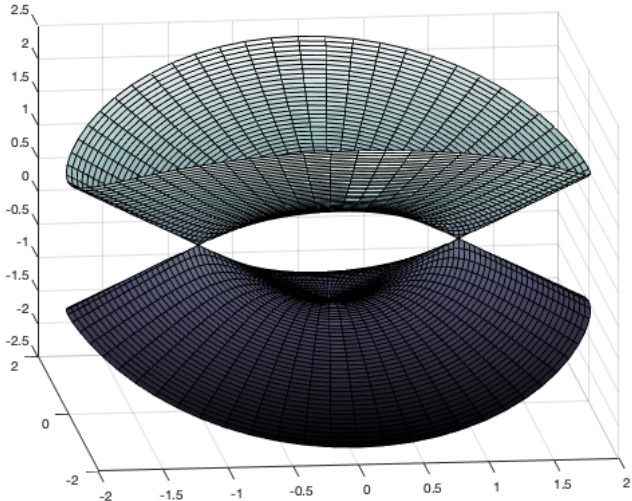


Figure 6: Band structure of two-valley linear Dirac Hamiltonian, $\Phi(\xi) = 1 - |\xi|$.

Another natural choice for Φ leading to a differential operator H_b is $\Phi(\xi) = \frac{1}{2}(\xi^2 - 1)$. In both cases, the valley at Dirac points $\xi = 1$ and $\xi = -1$ have topological indices given by 1 and -1 respectively. We will primarily focus on small highly oscillatory defects as a model for distribution of small defects.

Consider a semiclassical theory with $0 < \varepsilon \ll 1$ scaling near Dirac points so that the two valleys are separated by wavenumbers of order $2\varepsilon^{-1}$. We focus on a small energy window near $E = 0$ and thus analyze an equation of the form

$$\left(\Phi(\varepsilon D_x) \sigma_1 + \varepsilon D_y \sigma_2 + \lambda \frac{y}{\varepsilon} \sigma_3 + \varepsilon V(x, \frac{x}{\varepsilon}, \frac{y}{\varepsilon}) - \varepsilon E \right) \psi = 0. \quad (3.1)$$

In the absence of a domain wall ($\lambda = 0$) and perturbing potential ($V = 0$), assuming $|\Phi'(\pm 1)| = 1$, this system has a circular Fermi surface at small energies as is typical for Dirac points.

We consider a formal derivation in the limit $\varepsilon \ll 1$ of an inter-valley coupling model whose qualitative predictions will be confirmed by numerical simulations. While many steps can undoubtedly be justified more rigorously using methodology such as in [15], we will not do so here.

The domain wall $\lambda \frac{y}{\varepsilon} \sigma_3$ is assumed to be steep with $\lambda \gg 1$ as this prevents coupling between various confined modes in y . Introduce the microscopic variable $Y = y/\varepsilon$ and look for solutions of the form $\psi(Y = \frac{y}{\varepsilon}, x)$. Applied to such functions, (3.1) becomes

$$(D_Y \sigma_2 + \lambda Y \sigma_3 + \Phi(\varepsilon D_x) \sigma_1 + \varepsilon V(x, \frac{x}{\varepsilon}, Y) - \varepsilon E) \psi = 0. \quad (3.2)$$

When λ is large, then the two first terms dominate in the sense that

$$(D_Y \sigma_2 + \lambda Y \sigma_3) \phi_0(Y) = 0, \quad \phi_0(Y) = (\lambda \pi)^{-1/4} e^{-\frac{1}{2} \lambda Y^2} \cdot \frac{1}{\sqrt{2}} \begin{pmatrix} 1 \\ -1 \end{pmatrix},$$

while $D_Y \sigma_2 + \lambda Y \sigma_3$ applied to any other Hermite function provides a term of order $|\lambda| \gg 1$ formally much larger than the term $\Phi(\varepsilon D_x) \sigma_1$.

Decomposing $\psi(x, y, Y) = \phi_0(Y) \psi(x)$ for a scalar function $\psi(x)$ thus neglecting higher-order Hermite functions in Y , we obtain from (3.2) (multiplying by ϕ_0^T and integrating in Y) a reduced Hamiltonian for $\psi(x)$ given by

$$\left(-\Phi(\varepsilon D_x) + \varepsilon V(x, \frac{x}{\varepsilon}) - \varepsilon E \right) \psi = 0. \quad (3.3)$$

Here, $V(x, X) = (\phi_0(Y), V(x, X, Y) \phi_0(Y))_Y$. We also used that the current

$$(\phi_0, \sigma_1 \phi_0)_Y = -1.$$

In both cases, $(\cdot, \cdot)_Y$ is the usual inner product on $L^2(\mathbb{R}_Y; \mathbb{C}^2)$.

Define now multiscale functions $f(x, X = \frac{x}{\varepsilon})$ in the variable x so that D_x becomes $D_x + \varepsilon^{-1} D_X$. Then the multiscale operator is

$$-\Phi(D_X) + (-\Phi'(D_X) D_x + V(x, X) - E) \varepsilon + O(\varepsilon^2). \quad (3.4)$$

Going to the Fourier domain $X \rightarrow K$ we obtain

$$-\Phi(K) + (-\Phi'(K) D_x + \hat{V}(x, K) * -E) \varepsilon + O(\varepsilon^2). \quad (3.5)$$

Here $*$ is convolution in the Fourier variable K . To leading order we get

$$\Phi(K) \psi_0 = 0, \quad \text{i.e.,} \quad \psi_0 = \psi_+(x) \delta(K - 1) + \psi_-(x) \delta(K + 1). \quad (3.6)$$

The next order is

$$-\Phi(K)\psi_1 - \Phi'(K)D_x\psi_0 + \int \hat{V}(x, K - K')\psi_0(x, K')dK' - E\psi_0 = 0. \quad (3.7)$$

We thus find the coupled equations

$$-\Phi'(1)D_x\psi_+ + \hat{V}(x, 0)\psi_+ + \hat{V}(x, 2)\psi_- = E\psi_+ \quad (3.8)$$

$$-\Phi'(-1)D_x\psi_- + \hat{V}(x, 0)\psi_- + \hat{V}(x, -2)\psi_+ = E\psi_-. \quad (3.9)$$

This generates inter-valley coupling if by valleys we mean the wavenumbers close to $K = \pm 1$. Letting

$$H_2 = \begin{pmatrix} -\Phi'(1)D_x + \hat{V}(x, 0) & \hat{V}(x, 2) \\ \hat{V}(x, -2) & -\Phi'(-1)D_x + \hat{V}(x, 0) \end{pmatrix}, \quad (3.10)$$

we obtain the eigenproblem $H_2\psi = E\psi$, $\psi = (\psi_+, \psi_-)^T$, as a one-dimensional model incorporating valley coupling.

We now build a two-dimensional Hamiltonian that incorporates a domain wall and valley coupling. Generalizing the above Hamiltonian to include a y -dependent potential,

$$H_2^y = \begin{pmatrix} -\Phi'(1)D_x + \hat{V}(x, 0, y) & \hat{V}(x, 2, y) \\ \hat{V}(x, -2, y) & -\Phi'(-1)D_x + \hat{V}(x, 0, y) \end{pmatrix}, \quad (3.11)$$

we then define the 4×4 system

$$H_4 = D_y I_2 \otimes \sigma_2 + \lambda y I_2 \otimes \sigma_3 + H_2^y \otimes \sigma_1. \quad (3.12)$$

We choose this Pauli matrix representation such that H_4 is consistent with H_2 when V is y -independent. In particular, for e_\pm being the standard basis of \mathbb{R}^2 corresponding to valley index, $e_\pm \otimes \phi_0(y)$ are still in the kernel of the domain wall terms (first two terms), and $\phi_0(y)$ is an eigenfunction of σ_1 , meaning when V is y -independent the edge state eigenfunctions of H_2 naturally generalize to eigenfunctions of H_4 .

The operators in (3.10) and (3.12) are used for the numerical simulations of valley coupling effects.

Remark 1. Instead of $\varepsilon V(x, \frac{x}{\varepsilon})$, we could consider a larger-amplitude lower-frequency perturbation $V(x)$ in (3.1), another form of defect studied numerically in [24, 31]. Let us make a few brief remarks on this setting. In the semiclassical limit of large valley separation of order $2\varepsilon^{-1}$, we derive as above the one-dimensional semiclassical problem

$$(-\Phi(\varepsilon D_x) + V(x) - E)\psi = 0. \quad (3.13)$$

Consider the well-studied case $\Phi(\xi) = 1 - \xi^2$ for concreteness and see, e.g., [14] for an analysis of such semiclassical problems.

We may find to arbitrary algebraic accuracy in powers of ε solutions of the form

$$\psi(x) = \sum_{\pm} e^{iS_{\pm}(x)/\varepsilon} a_{\pm}(x; \varepsilon), \quad -\Phi(\partial_x S_{\pm}) + V(x) - E = 0. \quad (3.14)$$

The latter eikonal equation for S_{\pm} admits two solutions

$$S_{\pm}(x) = \pm \int_0^x (\Phi(0) + E - V(z))^{\frac{1}{2}} dz. \quad (3.15)$$

We assume $\Phi(0) + E - V(0) > 0$ so that propagating modes exist at x_0 with local wavenumber given by $\xi = \sqrt{\Phi(0) + E - V(0)}$ at the energy of interest E . Assuming $\Phi(0) + E - V(x)$ remains positive for all values of x , then ψ decomposes into two components $e^{iS_{\pm}(x)/\varepsilon}a_{\pm}(x; \varepsilon)$ that do not interact, resulting in extremely limited valley coupling.

Now, if $\Phi(0) + E - V(x) < 0$ is possible, then such values of x are forbidden energetically. Points x_0 such that $\Phi(0) + E - V(x_0) = 0$, assuming they are isolated (i.e., $V'(x_0) \neq 0$), are (caustic) turning points. Any signal arriving at x_0 from the area where $\Phi(0) + E - V(x) > 0$ will fully turn around so that the amplitudes a_{\pm} are now fully coupled. See, e.g., [18] for a detailed analysis of coupling (scattering) coefficients in various semiclassical settings.

We thus obtain a situation of extremely limited coupling if the eikonals S_{\pm} remain real valued, and full valley-coupling at turning points if the eikonals S_{\pm} may become complex-valued. We do not consider such a case further here.

3.2 Valley Conductivity

Now that we have constructed valley Hamiltonians H_2 and H_4 , we define valley contributions to conductivity so that we can study the separation of valleys under varying forms of perturbation. Recall we originally considered the conductivity object $\sigma_I = \text{Tr } i[H, P]\varphi'(H)$ with $P(x)$ a regularized Heaviside function. Here we consider H either H_2 or H_4 . However, for the two-valley system σ_I will always be 0 as when the two valleys are combined, we have a topologically trivial system.

We thus introduce a conductivity corresponding to a single valley so we can see the separation in valley contributions to conductivity. H_2 and H_4 are naturally structured to separate the valleys, making the definition of single valley conductivities reasonably straightforward. To construct, consider a wavefunction $(\psi_+, \psi_-)^t$ and define valley projector

$$P_+ = \begin{pmatrix} P & 0 \\ 0 & 0 \end{pmatrix}. \quad (3.16)$$

We consider the current on one side of the interface generated by P via the expression $(\psi_+, \dot{P}_+ \psi_+) = \text{Tr } \dot{P}_+ \psi_+ \otimes \psi_+^*$. If $U(t) = e^{-iHt}$ is the evolution of the Schrödinger equation, then

$$\dot{P}_+ := \partial_t(U(t)P_+U^*(t)) = U(t)[H, P_+]U^*(t). \quad (3.17)$$

We wish to rewrite including all wavefunctions corresponding to the edge. We pick $\varphi \in \mathfrak{S}(0, 1; -E_0, E_0)$ with $[-E_0, E_0]$ strictly in the bulk gap to capture spectral interface information. In particular, $\varphi'(H)$ captures all relevant modes. Decomposing the Hamiltonian H as (H_{ij}) for $1 \leq i, j \leq 2$ valley indices, we obtain

$$[H, P_+] = \begin{pmatrix} [H_{11}, P] & -PH_{12} \\ H_{21}P & 0 \end{pmatrix}$$

so that, with the same decomposition of $\varphi'(H)$,

$$[H, P_+]\varphi'(H) = \begin{pmatrix} [H_{11}, P]\varphi'_{11}(H) - PH_{12}\varphi'_{21}(H) & * \\ * & H_{21}P\varphi'_{12}(H) \end{pmatrix}.$$

The matrix trace therefore gives

$$\sigma_{I,+}(H) = \text{Tr } i[H, P_+]\varphi'(H) = \text{Tr } i[H_{11}, P]\varphi'_{11}(H) + \text{Tr } i[H_{21}, P]\varphi'_{12}(H). \quad (3.18)$$

The conductivity for the opposite valley is

$$\sigma_{I,-}(H) := \text{Tr } i[H, P_-]\varphi'(H) = \text{Tr } i[H_{22}, P]\varphi'_{22}(H) + \text{Tr } i[H_{12}, P]\varphi'_{21}(H).$$

For the above equation, H is first-order with an off-diagonal term, which is a multiplication operator in the case of H_2 and H_4 . This yields $[H_{21}, P] = 0$. Hence

$$\sigma_{I,+}(H) = \text{Tr } i[H_{11}, P]\varphi'_{11}(H), \quad \sigma_{I,-}(H) = \text{Tr } i[H_{22}, P]\varphi'_{22}(H). \quad (3.19)$$

3.3 Numerical example

First, we illustrate the deviation of the valley conductivity (3.18) from the quantized value ± 1 in the presence of a compactly supported potential V which couples the two valleys, see (3.1). Consider the leading ansatz (3.6) with

$$\psi_0(x) = e^{ix/\varepsilon}\psi_+(x) + e^{-ix/\varepsilon}\psi_-(x) \quad (3.20)$$

with the two Dirac cones at frequencies $\pm\varepsilon^{-1}$. Plugging the ansatz into (3.3), dividing by ε and multiplying by $e^{\pm ix/\varepsilon}$, we obtain, consistently with (3.8) after neglecting highly oscillatory terms $e^{\pm 2ix/\varepsilon}D_x\psi_{\pm}$ and $e^{\pm 2ix/\varepsilon}E$ that formally average to 0 according to (3.8), the following one-dimensional coupled Hamiltonian:

$$H_2^\varepsilon = \begin{pmatrix} -D_x & 0 \\ 0 & D_x \end{pmatrix} + V(x, x/\varepsilon) \begin{pmatrix} 1 & e^{-2ix/\varepsilon} \\ e^{2ix/\varepsilon} & 1 \end{pmatrix}, \quad (3.21)$$

so that to leading order $H_2^\varepsilon\psi = E\psi$ for $\psi = (\psi_+(x), \psi_-(x))^T$. We choose a two-scale potential of the form:

$$V(x, X) = V_0\chi(x)\cos(\omega X), \quad (3.22)$$

where $\chi(x)$ is a smooth, compactly supported function. Model (3.21) allows us to inspect the effects of the frequency of the fast component of the potential at a finite value of ε , such that some coupling is achieved at frequencies different from ± 2 , and homogenizes to (3.10) in the limit $\varepsilon \rightarrow 0$, when $\Phi'(\pm 1) = \pm 1$.

Here, we perform computations on the interval $[-50, 50]$ with periodic boundary conditions comparing all three models: (3.21) with $\varepsilon = 1$ and potential (3.22), and the models (3.10) (one-dimensional) and (3.12) (two-dimensional) obtained in the limit $\varepsilon \rightarrow 0$ with $\omega = 2$ with respective effective potentials described by

$$\widehat{V}(x, 0) = 0, \quad \widehat{V}(x, \pm 2) = \frac{V_0}{2}\chi(x) \quad \text{and} \quad \widehat{V}(x, 0, y) = 0, \quad \widehat{V}(x, \pm 2, y) = \frac{V_0}{2}\chi(x)\xi(y). \quad (3.23)$$

We choose functions $\chi(x)$ and $\xi(y)$ supported in the interval $[-20, 20]$ and $[-10, 10]$ and taking constant value 1 in the interval $[-10, 10]$ and $[-5, 5]$, respectively. Details of the pseudo-spectral discretization approach are postponed to section 5. The resulting conductivity σ^+ is plotted on Figure 7 as a function of x_0 , the center of the spatial switch function (3.16) and ω , the spatial frequency of the defect (3.22). In particular, we observe that at low frequencies ($\omega \approx 0$) the conductivity stays very close to the quantized value $\sigma^+ = 1$, while at $\omega = 2$, a maximum coupling between the valleys is achieved, locally reducing the conductivity measure by a large factor. Note that as $\varepsilon \rightarrow 0$, the limit model (3.10) shows coupling only at frequency $\omega = 2$. On the other hand, away from the defect the perturbation of the conductivity decays extremely fast regardless of the frequency ω .

As a second experiment, we compare the valley conductivity as a function of perturbation amplitude V_0 and energy E for Hamiltonians (3.10) and (3.12), that is by numerically computing the conductivity (3.18) when shifting the Hamiltonian as $H \rightarrow H - E$. We observe that the effect of the interval coupling term is to open a band gap at the Dirac cones $E = 0$, reducing the conductivity in a small range of energies around zero for both the one-dimensional, two-valley Hamiltonian (3.10) and the two-dimensional, two-valley Hamiltonian (3.12), showing excellent qualitative agreement between the two models.

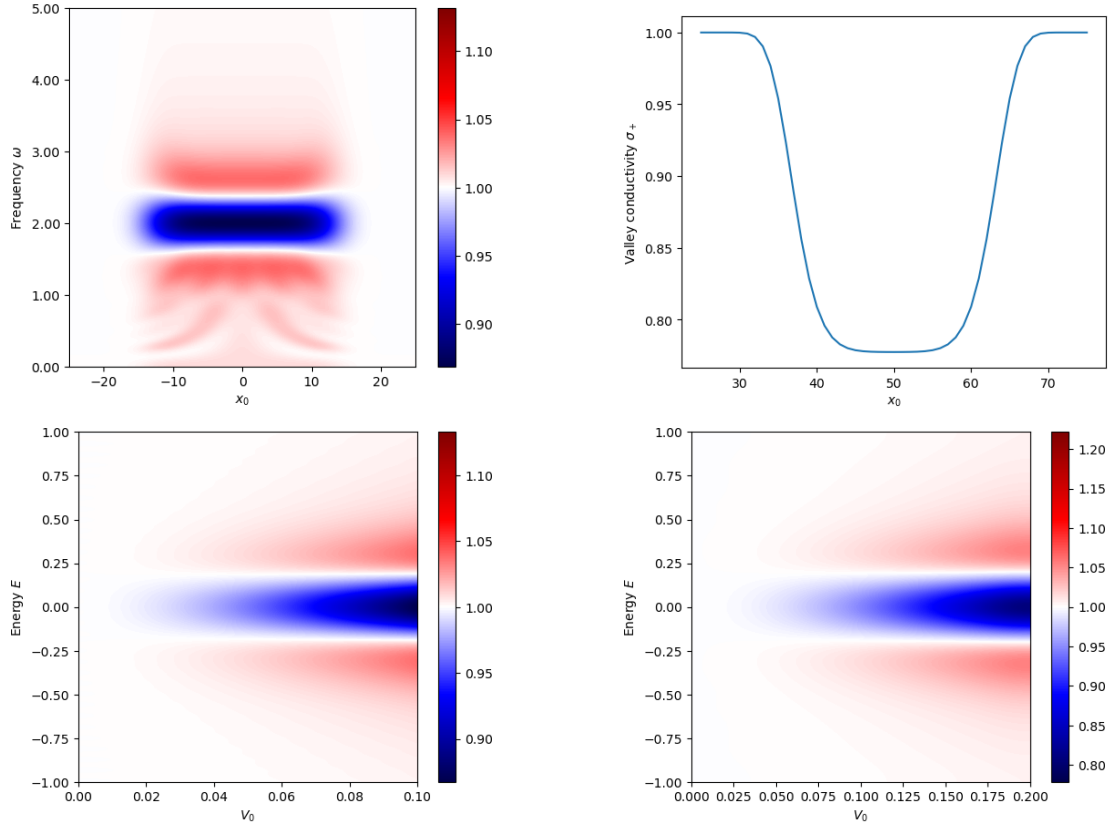


Figure 7: Valley conductivity $\sigma_{I,+}$ using the 1D models (3.21), (3.10) (left) and 2D model (3.12) (right), as a function of: spatial switch function center x_0 and frequency ω of the perturbation with amplitude $V_0 = 0.1$, using model (3.21) (top left); spatial switch function center x_0 , with a perturbation with amplitude $V_0 = 0.2$, using model (3.10) (top right); as a function of amplitude V_0 and energy E with frequency $\omega = 2$ and at $x_0 = 0$ for the 1D model (3.10) (bottom left) and 2D model (3.12) (bottom right).

3.4 One dimensional scattering theory

The conductivity $\sigma_{I,+}$ in Fig.7 (left) is close to 1 for ω away from 2 as expected from minimal valley coupling and close to 0 for $\omega = 2$, which is consistent with strong valley-coupling. For intermediate values of ω , we also observe a conductivity larger than 1. We now briefly consider a simplified one-dimensional model that exhibits such a behavior.

We revisit the one dimensional scattering problem (3.3), which we rewrite for $\Phi(\xi) = \frac{1}{2}(\xi^2 - 1)$ at $\varepsilon = 1$ and for a slightly different expression for the potential as the Helmholtz equation

$$(D_x^2 + V(x) - E)\psi = 0. \quad (3.24)$$

Assume $E = k^2 > 0$ so that when $V = 0$, we obtain $e^{\pm ikx}$ as standing (propagating) modes associated with each valley. We recall that $-D_x^2 = \partial_x^2$. In the presence of $V \neq 0$, these modes are coupled as described by (3.10) in the semiclassical regime. We wish to derive an explicit expression for valley conductivities using a scattering matrix formalism in the setting where $P' = \delta_{x_0}$ for $x_0 \in \mathbb{R}$ and where $\varphi' = \delta_E$ so that we estimate conductivities at fixed x_0 and energy E .

The two valley conductivities estimate the signals moving from left to right proportional to e^{ikx} and from right to left proportional to e^{-ikx} , respectively. Let us derive explicit expressions for those in terms of coefficients of scattering matrices. We wish to compute $\sigma_I^\pm[x_0, E]$ for \pm corresponding to left moving and right moving signals, respectively.

Consider (3.24) with $E = k^2$ and V compactly supported on $[x_L, x_R]$. We may then construct a standard scattering matrix such that $\psi(x < x_L) = e^{ikx} + R_+e^{-ikx}$ and $\psi(x > x_R) = T_+e^{ikx}$ for an incoming plane wave from the left of the support of V and such that $\psi(x < x_L) = T_-e^{-ikx}$ and $\psi(x > x_R) = e^{-ikx} + R_-e^{ikx}$ for an incoming plane wave from the right of the support of V .

Let us now decompose V into two subcomponents $V_{L,R}$ supported on $[x_L, x_0]$ and $[x_0, x_R]$, respectively when $x_L < x_0 < x_R$. For each subcomponent, define the scattering matrices

$$S^L = \begin{pmatrix} R_+^L & T_-^L \\ T_+^L & R_-^L \end{pmatrix}, \quad \text{and} \quad S^R = \begin{pmatrix} R_+^R & T_-^R \\ T_+^R & R_-^R \end{pmatrix},$$

where the coefficients R and T are interpreted as above.

These two matrices could be appropriately combined to construct a scattering matrix on the interval $[x_L, x_R]$ called S ; we do not need the details of this object.

Both S^L and S^R as well as S for the whole interval are unitary scattering matrix so that $SS^* = S^*S = I$. In particular, we observe that $|T_+| = |T_-|$ and $|R_+| = |R_-|$.

Consider the (unique) solution $\psi_L(x)$ of (3.24) at energy E equal to $e^{ikx} + Re^{-ikx}$ at x_L and let (u^L, v^L) be defined such that $\psi_L(x_0) = u^L e^{ikx_0} + v^L e^{-ikx_0}$. For this to hold, we formally assume that $V = 0$ at x_0 . Using the above matrices, we find

$$u^L = T_+^L + R_-^L v^L, \quad v^L = R_+^R u^L, \quad u^L = \frac{T_+^L}{1 - R_-^L R_+^R}, \quad v^L = \frac{R_+^R T_+^L}{1 - R_-^L R_+^R}.$$

Considering the solution equal to $e^{-ikx} + Re^{ikx}$ at x_R instead, we find for (u^R, v^R) the solution at x_0

$$v^R = T_-^R + R_+^R u^R, \quad u^R = R_-^L v^R, \quad v^R = \frac{T_-^R}{1 - R_-^L R_+^R}, \quad u^R = \frac{R_-^L T_-^R}{1 - R_-^L R_+^R}.$$

The above corresponding solutions $\psi_L(x)$ and $\psi_R(x)$ of (3.24) are orthogonal in the following sense. Assume an inner product on an interval $(-M, M)$ with $M \rightarrow \infty$ and hence normalized by $(2M)^{-\frac{1}{2}}$. So what happens on the support of V vanishes in the limit $M \rightarrow \infty$. The two solutions constructed above are of the form

$$e^{ikx} + R_+e^{-ikx} \quad \text{and} \quad T_+e^{ikx}$$

for the first solution on the left and right of the support of V and

$$T_-e^{-ikx} \quad \text{and} \quad e^{-ikx} + R_-e^{ikx}$$

for the second solution in the same sense. The inner product of these two functions for $k \neq 0$ is asymptotically given by $R_+^* T_- + T_+^* R_- = 0$. In other words, these two solutions correspond to two simple branches of absolutely continuous spectrum (parametrized by E) of the operator that live in orthogonal subsets of the Hilbert space.

The conductivity associated to the signal moving from left to right, which we associate with one of the valleys is given by the signal at x_0 moving to the right for the mixture of states having energy E . Thanks to the above orthogonality, the trace (sum over densities of orthogonal modes evaluated at x_0) is given by

$$\sigma_I^+[x_0, E] = |u^L|^2 + |u^R|^2 = \frac{|T_+^L|^2 + |R_-^L|^2 |T_-^R|^2}{|1 - R_-^L R_+^R|^2}.$$

The conductivity associated to the signal moving from the right to the left is given by

$$\sigma_I^-[x_0, E] = -(|v^L|^2 + |v^R|^2) = -\frac{|T_-^R|^2 + |R_+^R|^2|T_+^L|^2}{|1 - R_-^L R_+^R|^2}.$$

The sum of the nominators is given by

$$|T_+^L|^2 + (1 - |T_-^L|^2)|T_-^R|^2 - |T_-^R|^2 - (1 - |T_+^R|^2)|T_+^L|^2 = 0.$$

So, we do verify that $\sigma_I^+ + \sigma_I^- = 0$ as it should be for a globally topologically trivial material.

When x_0 is outside the support of V , say $x_0 \geq x_R$, then $T^R = 1$ and $R^R = 0$ so that

$$\sigma_I^+ = |T_+|^2 + |R_-|^2 = 1.$$

Similarly, σ_I^- would be equal to -1 outside of the support of V . It is therefore only on the support of the fluctuation V that we expect to observe spatial variations (in x_0) of the valley conductivities.

Let us consider a simplified setting. Assume that $x_0 = \frac{1}{2}(x_L + x_R)$ and that V is even about x_0 . Then by symmetry, $R_\pm^L = R_\mp^R$ and $T_\pm^L = T_\mp^R$ so that

$$\sigma_I^+ = \frac{|T_+^L|^2(1 + |R_-^L|^2)}{|1 - (R_-^L)^2|^2} = \frac{(1 - |R_-^L|^2)(1 + |R_-^L|^2)}{|1 - (R_-^L)^2|^2} = \frac{1 - |R_-^L|^4}{|1 - (R_-^L)^2|^2}.$$

Denoting $R_-^L = e^{i\theta}r$, we find

$$\sigma_I^+ = \frac{1 - r^4}{|1 - e^{2i\theta}r^2|^2} \approx 1 + 2 \cos 2\theta r^2,$$

for r small (corresponding to V small). The term $\cos 2\theta$ is positive or negative depending on the value of θ we obtain from the scattering theory. When $\theta = \frac{\pi}{2}$ so that R_-^L is purely imaginary, then we observe the largest drop in conductivity. When $\theta = 0$ however, we observe an increase in the local conductivity for small V before it decreases of large values of V . These observations are consistent with what we obtained in numerical simulations in Fig.7 and show that in the presence of intervalley-coupling, the conductivities associated to left-going and right-going modes are spatially dependent and hence not protected topologically.

As a concrete example, assume $V = V_0 \chi_{[-a, a]}$ as a barrier potential for the Left domain above leading to the computation of R_-^L . With $q = \sqrt{k^2 - V_0}$ assumed positive, standard calculations in the scattering theory of the one-dimensional Schrödinger equation then yield

$$R_-^L = \frac{V_0 \sin(2qa)e^{-2ika}}{(2k^2 - V_0) \sin(2qa) + 2ikq \cos(2qa)}.$$

When the width a is small, then to leading order in a , the phase of R_-^L is close to $e^{-i\frac{\pi}{2}}$. It may however, take arbitrary values for larger width a . Note that $R_-^L = 0$ when $2qa = n\pi$ for $n \in \mathbb{N}$.

4 Junction topology

This section addresses asymmetric transport through a junction in the xy -plane. We introduce a junction conductivity and compute it by means of a Fedosov-Hörmander formula, which extends what exists for the flat interface case [5, 25]. Pseudo-differential calculus will be used throughout; see Appendix B for notation and background.

Although our main result will apply to a more general class of models, we start with the example provided by region 2 from Figure 1. As shown, the region selects one vertex from the underlying periodic hexagonal

structure. We push all other vertices to infinity, so that our model consists of six slices alternating between AB and BA stacking. The corresponding junction Hamiltonian is

$$\text{Op}(\sigma) = H = \begin{pmatrix} \Omega I + D \cdot \sigma^{(\eta)} & \lambda U^*(x, y) \\ \lambda U(x, y) & -\Omega I + D \cdot \sigma^{(\eta)} \end{pmatrix},$$

where the notation on the left-hand side is defined in Appendix B, and $U(x, y) := \frac{1}{2}((1 + \tilde{m}(x, y))A + (1 - \tilde{m}(x, y))A^*)$. Here, $\tilde{m} \in \mathcal{C}^\infty$ is positive in regions of AB stacking, negative in regions of BA stacking, and zero on the boundaries between regions. We assume that $\tilde{m} \in \{-1, 1\}$ away from these boundaries.

To construct such a function \tilde{m} explicitly, define $f_\Theta : \mathbb{T} \rightarrow \mathbb{T}$ by $f_\Theta(\theta) = \sin(3\theta)$ and let $f \in \mathcal{C}^\infty(\mathbb{R}^2)$ such that $f(x, y) = rf_\Theta(\theta)$ for all $r \geq 1$, where (r, θ) are the polar coordinates corresponding to (x, y) . For concreteness, take $f(x, y) := \chi(r)rf_\Theta(\theta)$, where $\chi \in \mathfrak{S}(0, 1; \varepsilon, 1)$ and $0 < \varepsilon < 1$. An example of such a function f is plotted in Figure 8 (left panel). Since χ is smooth and vanishes near the origin, it is immediate that f is smooth. Let $m \in \mathfrak{S}(-1, 1)$ be monotonically increasing with $m(0) = 0$, and define $\tilde{m}(x, y) := m(f(x, y))$. This definition is consistent with the above constraints, as $f_\Theta > 0$ if and only if $2k\pi/3 < \theta < (2k + 1)\pi/3$ for some $k \in \{0, 1, 2\}$. Since m and all of its derivatives are bounded, it follows that $\sigma \in S_{1,0}^1$ with the right-hand side defined in Appendix B. Moreover, the structure of H (with $D \cdot \sigma^{(\eta)}$ on the diagonal and no other derivatives) implies the existence of a constant $c > 0$ such that $|\sigma_{\min}(x, y, \xi, \zeta)| \geq c\langle \xi, \zeta \rangle - 1$, where σ_{\min} is the smallest magnitude eigenvalue of σ , and for any vector u , we define $\langle u \rangle = \sqrt{1 + |u|^2}$. We see that when $f(x, y)$ is sufficiently large (resp. small), $\sigma = \sigma_+$ (resp. $\sigma = \sigma_-$), with $\text{Op}(\sigma_\pm) := H_\pm$ and H_\pm defined in section 2. By Appendix A, there exists $E > 0$ such that σ_\pm (equivalently H_\pm) has a spectral gap in the interval $(E_1, E_2) := (-E, E)$.

Analogous to (2.4) and [2, 4, 5, 25], we define the *junction conductivity* by

$$\sigma_I := \text{Tr } i[H, P]\varphi'(H), \quad (4.1)$$

where $\varphi \in \mathfrak{S}(0, 1; -E, E)$. The operator (of point-wise multiplication by) P is still a regularized indicator function, but it can no longer depend on only one variable. Indeed, for the operator on the right-hand side of (4.1) to be trace-class, it is necessary that ∇P decay to 0 along the level curves of f (otherwise, the symbol of $[H, P]\varphi'(H)$ would not decay in $\langle x, y \rangle$). This condition is satisfied if we set $P(x, y) = \chi_p(g(x, y))$, where $\chi_p \in \mathfrak{S}(0, 1)$ and $g \in \mathcal{C}^\infty(\mathbb{R}^2)$ such that $C_1\langle x, y \rangle \leq \langle f, g \rangle \leq C_2\langle x, y \rangle$ for some positive constants C_1 and C_2 . To construct such a function g explicitly, we can for example define $g_\Theta : \mathbb{T} \rightarrow \mathbb{T}$ by $g_\Theta(\theta) = \cos(\theta) + \cos(\pi/6) = \cos(\theta) + \sqrt{3}/2$ (note that $g_\Theta < 0$ if and only if $5\pi/6 < \theta < 7\pi/6$) and take $g(x, y) = \chi(r)rg_\Theta(\theta)$. See Figure 8 (center panel) for a plot of g . Since the zeros of f_Θ and g_Θ are disjoint, it is clear that the growth condition for $\langle f, g \rangle$ is satisfied. As we will show in detail below, the symbol of $\varphi'(H)$ (resp. $[H, P]$) decays rapidly in $\langle f(x, y), \xi, \zeta \rangle$ (resp. $\langle g(x, y) \rangle$), meaning that σ_I in (4.1) is well defined.

Due to the factor of χ in the definition of g , the level set $g^{-1}(0)$ is not a curve in the xy -plane. Still, there exists a smooth function $(x_0, y_0) : \mathbb{R} \rightarrow \mathbb{R}^2$ whose range separates the xy -plane into two regions, R_+ and R_- , such that $g \geq 0$ in R_+ and $g \leq 0$ in R_- . More specifically, we can take

$$(x_0(t), y_0(t)) = \begin{cases} (\frac{\sqrt{3}}{2}t, \frac{1}{2}t), & t \leq -1 \\ (-\frac{\sqrt{3}}{2}t, \frac{1}{2}t), & t \geq 1 \end{cases}$$

and smoothly connect (x_0, y_0) for $|t| < 1$ so that $g(x_0(t), y_0(t)) = 0$ for all $t \in \mathbb{R}$. For $(t, \xi, \zeta) \in \mathbb{R}^3$, define

$$\tau(t, \xi, \zeta) := \sigma(x_0(t), y_0(t), \xi, \zeta), \quad \tau_z := z - \tau. \quad (4.2)$$

The main result of this section is the following

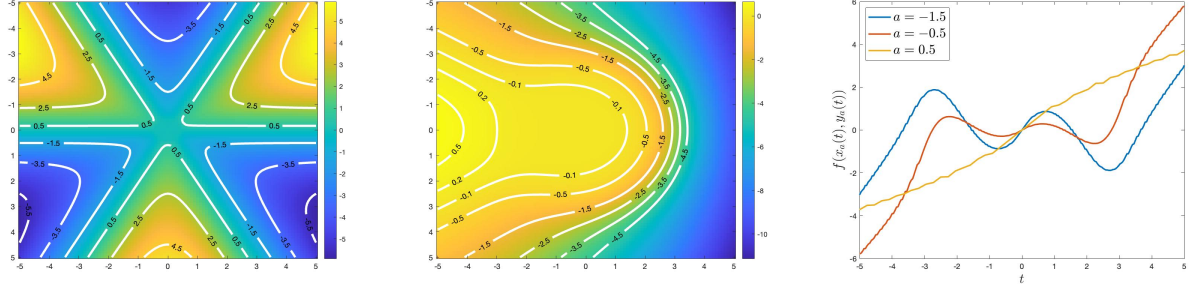


Figure 8: Plots of f (left) and g (center) in the xy -plane, with several level curves included. The right panel shows f evaluated along the level curves $\{g = a\}$ for three values of a . The curves are parametrized by the variable t , with the convention that $y_a(t) \rightarrow \pm\infty$ as $t \rightarrow \pm\infty$.

Theorem 4.1. *Let $\alpha \in (E_1, E_2)$ and let $R \subset \mathbb{R}^4$ be open and bounded with a piecewise smooth boundary ∂R . Assume R contains all points $(0, t, \xi, \zeta)$ where $\tau(t, \xi, \zeta)$ has an eigenvalue of α . Then for $z = \alpha + i\omega$, we have that*

$$2\pi\sigma_I = \frac{i}{24\pi^2} \int_{\partial R} \text{tr} \epsilon_{ijkl} \partial_i \tau_z \tau_z^{-1} \partial_j \tau_z \tau_z^{-1} \partial_k \tau_z \tau_z^{-1} \nu_l d\Sigma, \quad (4.3)$$

where ν is the unit vector (outwardly) normal to ∂R , $d\Sigma = d\Sigma(\omega, t, \xi, \zeta)$ is the Euclidean measure on ∂R , the variables are given by $(1, 2, 3, 4) = (\omega, \xi, \zeta, t)$, and ϵ_{ijkl} the anti-symmetric tensor with $\epsilon_{1234} = 1$.

We postpone the proof to Appendix B. Although motivated and introduced by the tBLG model from section 2, the above result applies to a large class of Hamiltonians H and corresponding energy intervals (E_1, E_2) ; see (H1) below. Moreover, the function g (and hence the regularized indicator function P) does not need to be defined as in the above example. Observe that the variable t in (4.3) takes on the role of y from [25, Theorem 4.1]. Thus Theorem 4.1 reduces the junction conductivity to the simpler flat-interface setting. Indeed,

$$\sigma_I(H) = \text{Tr } i[\tilde{H}, \tilde{P}]\varphi'(\tilde{H}),$$

where $\tilde{P}(x) = \tilde{P} \in \mathfrak{S}(0, 1)$ and \tilde{H} is the same as H but with $\tilde{m}(x, y)$ replaced by $m(f(x_a(y), y_a(y)))$ for any a . See Figure 8 (right panel) for plots of f along various level curves of g . Since

$$m(f(x_a(y), y_a(y))) =: m(y) = m \in \mathfrak{S}(-1, 1),$$

we recover exactly the conductivity given by Theorem 2.1.

If $P_j = \chi_p(g_j(x, y))$ for $j \in \{0, 1, 2\}$ with the g_j appropriately chosen to satisfy the growth condition for $\langle f, g \rangle$, then $\sigma_I(H; \sum_j P_j) = \sum_j \sigma_I(H; P_j)$. Thus if $g_j(x, y) = \chi(r)rg_{j\Theta}(\theta)$ with $g_{j\Theta} = \cos(\theta - 2\pi j/3) + \cos(\pi/6)$, then the $2\pi/3$ -rotational symmetry of the tBLG Hamiltonian implies that $\sigma_I(H; \sum_j P_j) = 3\sigma_I(H; P_0)$. In words, the superposition of three appropriately chosen regularized indicator functions increases the conductivity by a factor of 3. This makes perfect sense, as the conductivity is now measured through three distinct regions ($\text{supp } \nabla P_j$ for $j = 0, 1, 2$), each of which contributes the same value of η/π .

The rest of this section has three objectives. First, we provide the full class of operators H and P to which Theorem 4.1 applies. We then list several results addressing the stability of σ_I and regularity of the involved operators, in parallel with [25, section 3]. While interesting in their own right, these results are also

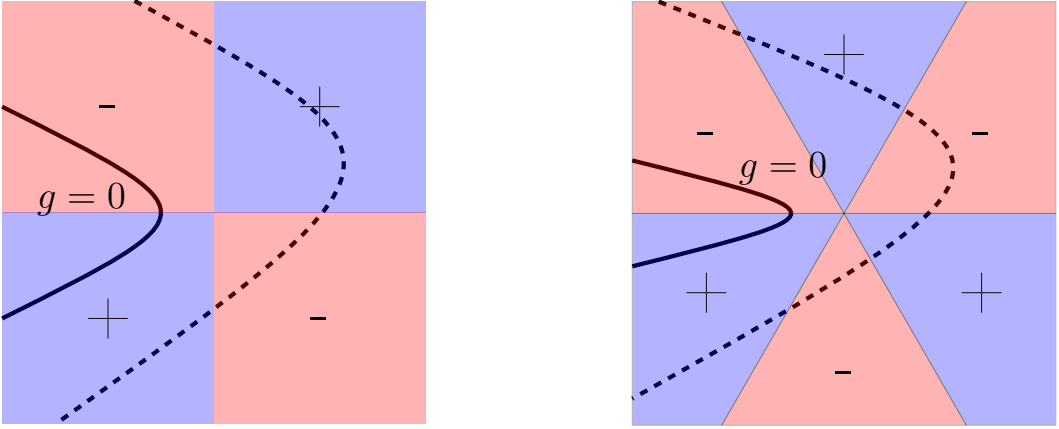


Figure 9: Illustrations of σ in the xy -plane for $k = 2$ (left) and $k = 3$ (right). The labels \pm indicate the sign of f . Two example level curves $\{g = 0\}$ are presented in each case (solid and dashed curves), for some arbitrary choices of g satisfying the appropriate assumptions. The scale of this picture is much smaller than 1, so that we are not in the region where $g(r, \theta) = rg_\Theta(\theta)$.

used in the proof of Theorem 4.1 (see Appendix B). Finally, we apply Theorem 4.1 to 2×2 Dirac models which are also the subject of section 5.

Let us introduce some notation. As above, the Hamiltonians H act on $\mathcal{H} := L^2(\mathbb{R}^2) \otimes \mathbb{C}^n$. We label the spatial coordinates $(x, y) \in \mathbb{R}^2$ and the corresponding dual variables $(\xi, \zeta) \in \mathbb{R}^2$. Given a function $u \in \mathcal{C}^\infty(\mathbb{R}^2)$, a matrix-valued function A , fixed matrices A_1 and A_2 , and fixed constants $c_1 < c_2$, we write $A \in \mathfrak{S}(A_1, A_2; c_1, c_2; u)$ to mean that

$$A = \begin{cases} A_1, & u \leq c_1 \\ A_2, & u \geq c_2 \end{cases}.$$

We let $\mathfrak{S}(A_1, A_2; u)$ denote the union of $\mathfrak{S}(A_1, A_2; c_1, c_2; u)$ over all $-\infty < c_1 < c_2 < \infty$. If $A = A(\alpha)$ is a function of just one variable, then we define $\mathfrak{S}(A_1, A_2; c_1, c_2) := \mathfrak{S}(A_1, A_2; c_1, c_2; \alpha)$ and $\mathfrak{S}(A_1, A_2) := \mathfrak{S}(A_1, A_2; \alpha)$. Note that if $A(x, y) = \chi_A(u(x, y))$ for some $\chi_A \in \mathfrak{S}(A_1, A_2)$, then $A \in \mathfrak{S}(A_1, A_2; u)$.

Let (r, θ) denote the polar coordinates for (x, y) . Fix $k \in \mathbb{N}$ and let $\Theta_k \subset [0, 2\pi)$ be any set containing $2k$ elements. Let $f_\Theta \in \mathcal{C}^\infty(\mathbb{T})$ such that $f_\Theta(\theta) = 0$ if and only if $\theta \in \Theta_k$, and $f'_\Theta(\theta) \neq 0$ whenever $\theta \in \Theta_k$. This means f_Θ changes sign across every point in Θ_k and is bounded away from 0 for all θ away from Θ_k . Let $f \in \mathcal{C}^\infty(\mathbb{R}^2)$ such that $f(x, y) = f(r, \theta) := rf_\Theta(\theta)$ whenever $r \geq 1$. We assume the following:

(H1) Let $H = \text{Op}(\sigma)$ be a symmetric pseudo-differential operator, with σ independent of h . Suppose $\sigma \in S_{1,0}^m$ for some $m \in \mathbb{N}$, and $|\sigma_{\min}(x, y, \xi, \zeta)| \geq c|\xi, \zeta|^m - 1$ for some $c > 0$. Suppose there exist values $-\infty < E_1 < E_2 < \infty$ and symbols $\sigma_\pm \in S_{1,0}^m$ independent of (x, y) with no spectrum in (E_1, E_2) , such that $\sigma(\cdot, \cdot, \xi, \zeta) \in \mathfrak{S}(\sigma_-(\xi, \zeta), \sigma_+(\xi, \zeta); f)$ for all $(\xi, \zeta) \in \mathbb{R}^2$.

By [9, 20], we know (H1) implies that $H : \mathcal{D}(H) \rightarrow \mathcal{H}$ is self adjoint with $\mathcal{D}(H) = \mathcal{H}^m$ (and the right-hand side the standard Hilbert space of functions with square-integrable derivatives up to order m).

For $h \in (0, 1]$, define $H_h := \text{Op}_h(\sigma)$. Let $\{\theta_1, \theta_2\} \subset \mathbb{T}$ such that $\theta_1, \theta_2 \notin \Theta_k$. Let $g_\Theta \in \mathcal{C}^\infty(\mathbb{T})$ such that $g_\Theta(\theta) = 0$ if and only if $\theta \in \{\theta_1, \theta_2\}$, and $g'_\Theta(\theta_j) \neq 0$ for $j \in \{1, 2\}$. Let $g \in \mathcal{C}^\infty(\mathbb{R}^2)$ such that $g(x, y) = g(r, \theta) = rg_\Theta(\theta)$ for all $r \geq 1$. It follows that there exists a smooth function $(x_0, y_0) : \mathbb{R} \rightarrow \mathbb{R}^2$ with

$\lim_{|t| \rightarrow \infty} |(x_0(t), y_0(t))| = \infty$ and whose range separates the xy -plane into two regions, R_+ and R_- , such that $g \geq 0$ in R_+ . One can for example take a curve contained in $\{g = 0\}$, in which case $(x_0(t), y_0(t)) = (\beta_1 t, \beta_2 t)$ for all $|t|$ sufficiently large, with the constants β_1 and β_2 depending only on $\operatorname{sgn} t$. Our convention is that R_+ be on the *right* side of the curve defined by (x_0, y_0) as t increases. That is, if you were to move along the curve with t increasing, then R_+ would be on your right.

Let $\varphi \in \mathfrak{S}(0, 1; E_1, E_2)$ and $P \in \mathfrak{S}(0, 1; g(x, y))$. We now adapt the results from [25, section 3] to the setting of this paper, starting with the following regularity result.

Proposition 4.2. *Suppose $H = \operatorname{Op}_1(\sigma)$ satisfies (H1), define*

$$H_h := \operatorname{Op}_h(\sigma(x, y, \xi, \zeta)) \text{ for } 0 < h \leq 1, \quad (4.4)$$

and let $\Phi \in \mathcal{C}_c^\infty(E_1, E_2)$. Then for all $P \in \mathfrak{S}(0, 1; g(x, y))$, we have

$$\Phi(H_h) \in \operatorname{Op}_h(S(\langle f(x, y), \xi, \zeta \rangle^{-\infty})) \quad \text{and} \quad [H_h, P]\Phi(H_h) \in \operatorname{Op}_h(S(\langle x, y, \xi, \zeta \rangle^{-\infty})).$$

Next we have that the junction conductivity is independent of which $P \in \mathfrak{S}(0, 1; g(x, y))$ we choose.

Proposition 4.3. *If $P, \tilde{P} \in \mathfrak{S}(0, 1; g(x, y))$, then $\operatorname{Tr} i[H, P]\varphi'(H) = \operatorname{Tr} i[H, \tilde{P}]\varphi'(\tilde{H})$.*

To further motivate and explain this result, recall that our model is of two types of materials (+ and $-$) that are smoothly glued together at a junction. See Figure 9 for two examples, where we assume for concreteness that P transitions from 0 to 1 in the vicinity of $\{g = 0\}$. The solid curve (in both panels) can see only a transition from σ_+ to σ_- , while the dashed level curves contain multiple transitions ($+\rightarrow-\rightarrow+\rightarrow-$ for the left panel and $+\rightarrow-\rightarrow+\rightarrow-\rightarrow+\rightarrow-$ for the right panel). As expected, the conductivity only cares about the “starting” and “ending” topology along the level curve and is unaffected by oscillations in between. This is analogous to invariance of σ_I with respect to compactly supported perturbations $V(y)$ in the case where $f = y$ and $g = x$ [25].

Finally, we present three stability results.

Proposition 4.4. *Suppose H and \tilde{H} both satisfy (H1), define $V := \tilde{H} - H$ and take φ as above. Let $\Phi_0 \in \mathcal{C}_c^\infty(E_1, E_2)$ such that ¹ $\varphi' \in \mathcal{C}_c^\infty(\{\Phi_0 = 1\}^\circ)$. If $\Phi_0(H)V(i - \tilde{H})^{-1}$ and $(i - H)^{-1}V\Phi_0(\tilde{H})$ are trace-class, then $\sigma_I(H) = \sigma_I(\tilde{H})$.*

Corollary 4.5. *Suppose H satisfies (H1) and $V(x, y) \in \mathcal{C}_c^\infty(\mathbb{R}^2) \otimes \mathbb{M}_n$. Then $\sigma_I(H) = \sigma_I(H + V)$.*

Proposition 4.6. *If $H = \operatorname{Op}(\sigma)$ satisfies (H1) with $\sigma(x, y, \xi, \zeta) = \tilde{\sigma}(f(x, y), \xi, \zeta)$ for some $\tilde{\sigma} \in \mathcal{C}^\infty(\mathbb{R}^3) \otimes \mathbb{M}_n$, then $\sigma_I(H_h)$ is independent of $h \in (0, 1]$.*

The Fedosov-Hörmander formula (4.3) applies to any Hamiltonian H satisfying the assumptions of Proposition 4.6. See Appendix B for the proof, which uses the independence of σ_I with respect to h to derive the formula in the semi-classical limit [5, 25]. We omit the proofs of Propositions 4.2–4.6, as they are almost identical to the ones in [25, section 3]. One must simply replace the spatial variables (x, y) by the functions $(g(x, y), f(x, y))$, and use that $c\langle x, y \rangle \leq \langle g, f \rangle \leq C\langle x, y \rangle$ for some $0 < c < C$.

We conclude this section with an application of Theorem 4.1 to 2×2 Dirac Hamiltonian given by

$$H = D_x \sigma_1 + D_y \sigma_2 + \tilde{m}(x, y) \sigma_3, \quad (4.5)$$

where $\tilde{m}(x, y) = m(f(x, y))$ for some $m \in \mathfrak{S}(0, 1)$, and

$$f(r, \theta) = \chi(r) r f_\Theta(\theta), \quad \chi \in \mathfrak{S}(0, 1; \varepsilon, 1), \quad f_\Theta(\theta) = \sin(k\theta)$$

¹We write U° to mean the interior of U .

for some $0 < \varepsilon < 1$ and $k \in \mathbb{N}_+$. Note that when $k = 1$, we recover the setting of a flat interface analyzed in detail in [2, 3, 4, 5, 25], while $k = 3$ yields the same hexagonal structure analyzed at the beginning of this section.

Take $P(x, y) = \chi_p(g(x, y))$ for $\chi_p \in \mathfrak{S}(0, 1)$, where $g(x, y) = g(r, \theta) = \chi(r)rg_\Theta(\theta)$ and $g_\Theta(\theta) = \cos(\theta - \theta_1) - \cos(\theta_0)$, for some $0 < \theta_0 < \pi$ and $-\frac{\pi}{k} < \theta_1 < \frac{\pi}{k}$ satisfying

$$\theta_+ \notin \Theta_k, \quad 2\pi - \theta_+ \notin \Theta_k, \quad \Theta_k = \left\{ \frac{j}{k\pi} : j \in \mathbb{Z} \right\}, \quad \theta_+ := \theta_0 + \theta_1.$$

This way, the zeros of g_Θ and f_Θ are disjoint. Indeed, $g_\Theta(\theta) = 0$ if and only if $\cos(\theta - \theta_1) = \cos(\theta_0)$, which occurs exactly when $\{\theta + 2\pi j : j \in \mathbb{Z}\} \cap \{\theta_+, 2\pi - \theta_+\} \neq \emptyset$. It follows that $\tau(t, \xi, \zeta) = \xi\sigma_1 + \zeta\sigma_2 + \mu(t)\sigma_3$ for some $\mu \in \cup_{\varepsilon_1, \varepsilon_2 \in \{-1, 1\}} \mathfrak{S}(\varepsilon_1, \varepsilon_2)$, where the ε_j are determined by θ_0 and θ_1 . We have reduced the problem to computing the interface conductivity for the translation-invariant 2×2 Dirac system [2, 5, 25], and hence $2\pi\sigma_I = \frac{1}{2}(\varepsilon_1 - \varepsilon_2)$. For the case $(k, \theta_1) = (3, 0)$ which is analyzed numerically in the following section, we have

$$2\pi\sigma_I = \begin{cases} -1, & 0 < \theta_0 < \pi/3 \\ 1, & \pi/3 < \theta_0 < 2\pi/3 \\ -1, & 2\pi/3 < \theta_0 < \pi \end{cases}.$$

If g from Figure 9 were to have the above form, then $\theta_1 = 0$ and θ_0 would be the angle between [the line making up the top of the level curve $\{g = 0\}$] and [the positive x -axis]. So $\pi/2 < \theta_0 < \pi$ and $2\pi/3 < \theta_0 < \pi$ for the left and right panels, respectively.

5 Numerical Simulations

We now present results of numerical simulations illustrating the stability of the interface and junction conductivities analyzed in the preceding sections. We augment these spectral results with simulations of wavepackets propagating across the junction considered in section 4 (case $k = 3$ in Fig. 9).

5.1 Methods and Discretization

All computations are conducted on a finite interval of size L for one-dimensional problems such as (3.10) (see section 3.3) or a rectangular domain of size $L_x \times L_y$ for two-dimensional problems such as conductivities for the Hamiltonian (3.12) or (4.5), equipped with periodic boundary conditions. We use a pseudo-spectral discretization where all functions are approximated using truncated Fourier series:

$$u(x) = \sum_{k=-K}^K \widehat{u}_k e^{2i\pi kx/L} \quad \text{or} \quad u(x, y) = \sum_{k=-K_x}^{K_x} \sum_{l=-K_y}^{K_y} \widehat{u}_{k,l} e^{2i\pi kx/L_x + 2i\pi ly/L_y},$$

such that derivation operators are represented as diagonal matrices. Pointwise multiplication operators such as $Vu(x) = v(x)u(x)$ are computed using Fourier interpolation on a uniform real-space grid of size $3(K+1)$ in the one-dimensional case and $3(K_x+1) \times 3(K_y+1)$ in the two-dimensional one employing the discrete Fourier transform \mathcal{F} , avoiding the aliasing of products for small values of K and sharp or highly oscillatory mass or potential profiles $m(x, y), v(x, y)$.

Computations of conductivities using finite domains are accomplished using the approximation

$$2\pi\tilde{\sigma}(H) = 2\pi \operatorname{Tr} iQ[H, P]\phi'(H), \tag{5.1}$$

where $P = p(x, y)$ and $Q = q(x, y)$ are pointwise multiplication operators where, as before, $p(x, y)$ is a spatial smooth switch function across a certain contour, and $q(x, y)$ is a spatial filter designed to mask the boundaries which may host artificial, unwanted domain walls (necessary to have space-dependent coefficients such as $m(x, y)$ remain smoothly connected across the periodic boundaries of the torus). More precisely, we set here:

$$p_{x_0, \delta}(x, y) = \begin{cases} 1, & \max \{x - x_0, -\cos(\theta)(y - L_y/2) \pm \sin(\theta)(x - x_0 - L_x/4)\} \geq \delta, \\ 0, & \max \{x - x_0, -\cos(\theta)(y - L_y/2) \pm \sin(\theta)(x - x_0 - L_x/4)\} \leq -\delta, \end{cases}$$

and

$$q_\delta(x, y) = \begin{cases} 1, & \max \{|x - L_x/2| - L_x/4, |y - L_y/2| - 3L_y/8\} \leq -\delta, \\ 0, & \max \{|x - L_x/2| - L_x/4, |y - L_y/2| - 3L_y/8\} \geq \delta, \end{cases}$$
(5.2)

such that δ is a small parameter controlling the width of transition regions, $\theta = \pi - \frac{\pi}{12}$ is as in Section 4 and x_0 is the abscissa at which the support of $\nabla p_{x_0, \delta}$ crosses the horizontal axis: see Figure 10 for such a profile. Valley-projected numerical conductivities $\tilde{\sigma}_\pm$ are defined similarly (3.18).

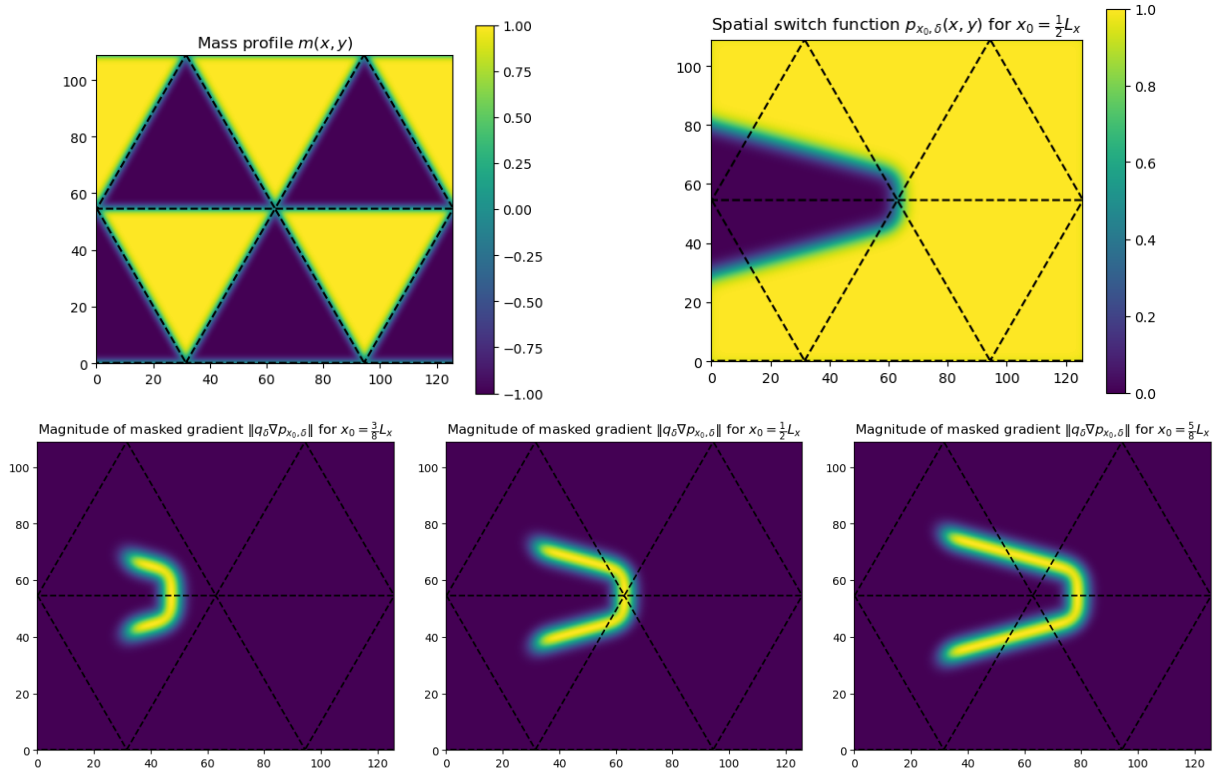


Figure 10: Top left: mass profile $m(x, y)$ yielding a three-fold symmetric topological junction. The contour $m(x, y) = 0$ is highlighted in dashed black line. Top right: spatial switch function $p_{x_0, \delta}(x, y)$ for $x_0 = L_x/2$ used in the computation of the conductivity (5.1). Bottom row: magnitude profiles of the gradient of the spatial switch function $\nabla p_{x_0, \delta}(x, y)$ multiplied by the filter $q_0(x, y)$ (5.2) for the three values (from left to right) $x_0 = 3L_x/8, L_x/2, 5L_x/8$ presented in Table 1.

Practically, the evaluation of (5.1) is achieved by direct diagonalization of the discretized Hamiltonian H , resulting in the sum-over-states formula:

$$2\pi\tilde{\sigma}(H) = 2\pi \sum_j \phi'(\lambda_j) \left\langle u_j \left| Q_\delta \begin{pmatrix} 0 & \partial_x p_{x_0, \delta} - i\partial_y p_{x_0, \delta} \\ \partial_x p_{x_0, \delta} + i\partial_y p_{x_0, \delta} & 0 \end{pmatrix} \right| u_j \right\rangle,$$

where λ_j , u_j are the eigenvalues and eigenvectors of H and the scalar product is evaluated by quadrature on the uniform real-spaced grid discussed earlier.

The spectral accuracy of the numerical conductivity (5.1) using our spectral discretization scheme can be established rigorously by observing that the relevant edge states vanish exponentially fast in the bulk. We do not pursue this analysis here and refer to [25] for the case of a single straight domain wall for elliptic partial differential operators, including the massive Dirac operator.

5.2 Invariant Calculations for Junctions

As a first numerical experiment illustrating the results of Section 4, we compute the conductivity in a hexagonal junction setup as in region 2 from Figure 1, i.e. a vertex with three-fold symmetry with the topology as in Figure 9. Specifically, our choice of spatial projector (5.2) with $\theta = \pi - \frac{\pi}{12}$ corresponds to a function g whose level set $g^{-1}(0)$ fully encloses only the left horizontal branch of the boundary set $m^{-1}(0)$, i.e. the negative real axis.

Results from Section 4 predict that the quantity $2\pi\sigma_I$ takes the value 1 independently of the exact choice of such a spatial projector, in particular whether $x_0 < L_x/2$ and the level set $g^{-1}(0)$ intersects the negative real axis only, or $x_0 > L_x/2$ and it crosses the other five boundaries. Our numerical computations, presented in Table 1, are consistent with the theory, with the converged results ($N = 64$) agreeing up to four digits of accuracy with the predicted value.

Table 1 also illustrates the stability and efficiency of our pseudo-spectral discretization approach. For all three choices of parameter x_0 , we note the exponential convergence of the computed conductivity with the frequency cutoff parameter N , consistent with the robustness of the conductivity demonstrated in earlier sections. Numerical experiments (not presented) also indicate fast exponential convergence in the size of the domain $L_x \times L_y$, consistent with the exponential localization of eigenmodes in the energy window of interest around boundaries of interest as well as artificial domain walls induced by periodization.

	$N = 8$	$N = 16$	$N = 32$	$N = 64$
$x_0 = 3L_x/8$	0.36144	0.92310	0.99923	0.99983
$x_0 = L_x/2$	0.53574	0.72033	0.99612	0.99997
$x_0 = 5L_x/8$	0.05648	0.88647	0.99901	0.99993

Table 1: Conductivity values (5.1) computed for different values of the spatial switch function center x_0 along the x -axis, and discretization parameter $N = K_x = K_y$.

5.3 Wavepacket Propagation through Junctions

Next, we study numerically the time-domain propagation of wavepackets through a hexagonally symmetric junction given by the same mass profile as plotted in Figure 10. Let us note that the stable topological invariants presented in Section 4, which can be interpreted as counting the net number of modes or currents traveling in certain directions along the interfaces [23, 3, 2], only partly predict the dynamics of localized wavepackets traveling across a junction. In particular, the sign of the conductivity identifies certain branches of the interface $m^{-1}(0)$ as incoming channels on which net propagation of current is towards the junction,

while on others current is outgoing, directed outwards from the junction (with the sum of current on all channels always being zero). On the other hand, the steady-state current generated by the state $\phi'(H)$ is equally distributed between all channels, and does not allow to distinguish how the current 'originating' from one of the incoming channels distributes itself.

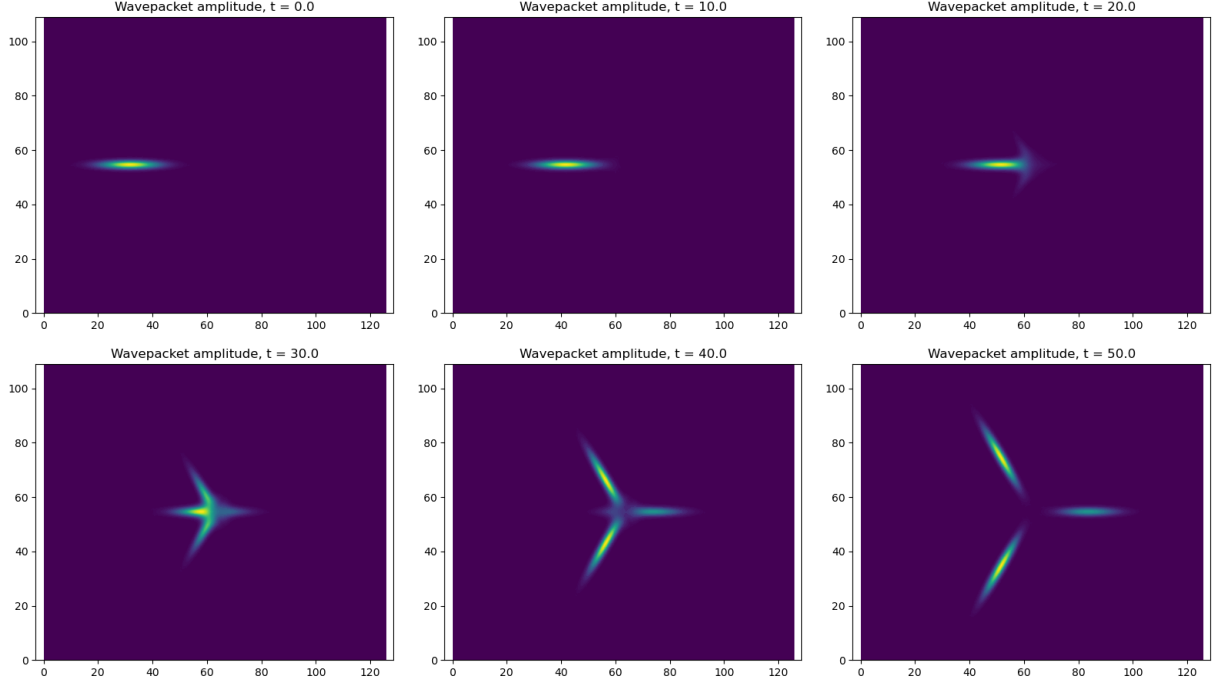


Figure 11: Scattering of a wavepacket incoming from the left along a horizontal branch towards a hexagonal cross, with a rotationally symmetric mass profile.

Semiclassical analysis, in the case of non-intersecting, straight or curved interfaces, shows that for Dirac operators such as the one considered here (4.5), these currents have a local interpretation via the construction of long-lived localized wavepackets travelling unidirectionally [6], with some dispersion due to the curvature of the interface. Hence, wavepackets travelling along an interface towards the junction are expected to scatter into any number wavepackets travelling on the outgoing channels.

While such rigorous analysis has not been carried out in the case of junctions, our numerical simulations of such scattering across a hexagonal junction show that a Gaussian wavepacket, initially travelling along the incoming channel supported by the horizontal edge to the left of the junction, splits three-fold at the intersection along the three outgoing branches of the junction: see snapshots of the evolution presented in Figure 11. More precisely, an initial Gaussian packet is prepared at $t = 0$ on the left horizontal branch which forms an incoming channel towards the intersection, and we compute its time evolution until $t = 50$ where the packet has completed its travel through the intersection. In contrast to the numerical results presented in [6], we observe remarkably little dispersion of the packet despite the sharp turns in the direction of propagation.

As mentioned above, the topology measured by the quantized junction conductivity, while heuristically linked to the robustness and stability of the propagating edge modes, does not distinguish between channels and thus does not constrain the entries of the scattering matrix between modes supported by incoming and outgoing channels. We observe on Figure 11 that the wavepacket does not split equally between all three

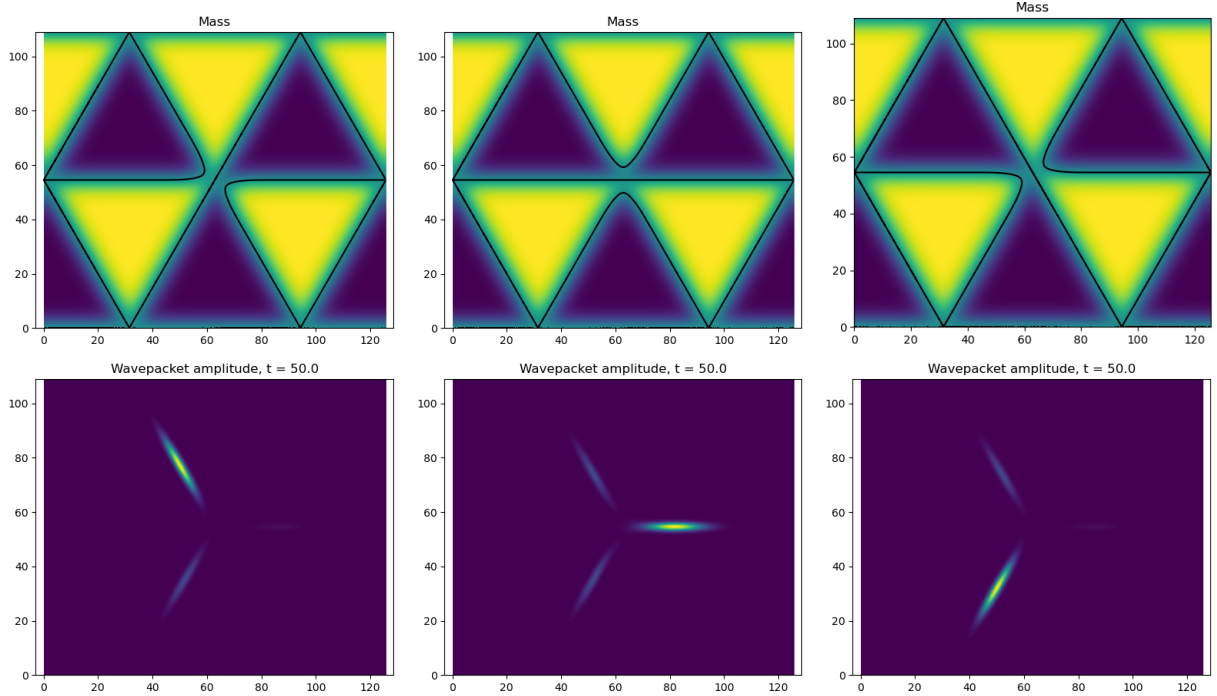


Figure 12: Scattering of a wavepacket through a hexagonal cross with broken symmetry profiles, allowing to steer a wavepacket incoming from the left towards any outgoing branch.

branches, with a smaller amount travelling straight across the intersection.

To illustrate the absence of stability of the scattering with respect to perturbations, we present in Figure 12 the final state of simulations with the same initial wavepacket as in Figure 11, but where a small, local perturbation of the mass term breaks the rotational symmetry: namely we set

$$m(x, y) = m_0(x, y) - \frac{1}{4} \exp \left(-\frac{(x - L_x/2)^2 + (y - L_y/2)^2}{2\sigma^2} \right) \begin{pmatrix} \sin(\theta_m) \\ \cos(\theta_m) \end{pmatrix} \cdot \begin{pmatrix} x - L_x/2 \\ y - L_y/2 \end{pmatrix},$$

where $m_0(x, y)$ is the symmetric mass profile as in Figure 10, $\sigma = 5$ is a width parameter and $\theta_m = 2\pi/3, 0, -2\pi/3$ respectively from left to right. These simulations indicate that the scattering can be completely manipulated by such local mass perturbations, and is not a protected property of the system: indeed, the wavepacket can be steered towards any of the three outgoing branches.

6 Conclusion

We consider continuum partial (and pseudo) differential models of twisted bilayer graphene (tBLG) that accurately describe macroscopic transport properties in tBLG. The twisted layers generate a macroscopic triangular moiré pattern separating regions of AB and BA stacking as shown in Fig. 1.

The primary focus of this work is to analyze the asymmetric transport observed at the interface between insulating AB and BA stackings (region 1 in Fig. 1) and at the junctions of the triangular pattern (region 2 in Fig. 1).

Asymmetry is quantified by observables of the system referred to as conductivities. A familiar *line conductivity* analyzed for such pseudo-differential equations in [2, 4, 5, 25] describes the asymmetry in region 1. We adapted the derivations in [7] in the context of Floquet topological insulators to compute the line conductivity and show that it took integral values by means of a bulk-interface correspondence.

The aforementioned asymmetry takes opposite values in each valley of the problem so that asymmetric transport is observed only when inter-valley coupling is negligible. We presented a class of simplified Hamiltonians modeling such valley coupling. We defined partial line conductivities for the two valleys and showed formally and numerically that these conductivities were no longer quantized and hence no longer stable with respect to perturbations.

Finally, to constrain transport across junctions in region 2 of Fig. 1, we introduced a notion of *junction conductivity* defined for a large class of domain walls modeling the insulating regions near the junction and for a large class of (pseudo-)differential operators including the Dirac operators modeling tBLG. Adapting techniques developed in [25], we demonstrated that the junction conductivity was indeed quantized and obtained by a Fedosov-Hörmander formula generalizing that for line conductivities. Numerical simulations of junction conductivities and other transport phenomena for a simple model of Dirac equation confirmed the theoretical predictions.

Acknowledgments

This research was partially supported by the National Science Foundation, Grants DMS-1908736, DMS-1819220 and EFMA-1641100.

References

- [1] M. Andelković, L. Covaci, and F. M. Peeters. Dc conductivity of twisted bilayer graphene: Angle-dependent transport properties and effects of disorder. *Phys. Rev. Materials*, 2:034004, Mar 2018.
- [2] G. Bal. Continuous bulk and interface description of topological insulators. *Journal of Mathematical Physics*, 60(8):081506, 2019.
- [3] G. Bal. Topological protection of perturbed edge states. *Communications in Mathematical Sciences*, 17(1):193–225, 2019.
- [4] G. Bal. Topological charge conservation for continuous insulators, 2021.
- [5] G. Bal. Topological invariants for interface modes. *To appear in Communications in Partial Differential Equations*, 2022.
- [6] G. Bal, S. Becker, A. Drouot, C. F. Kammerer, J. Lu, and A. Watson. Edge state dynamics along curved interfaces. *arXiv preprint arXiv:2106.00729*, 2021.
- [7] G. Bal and D. Massatt. Multiscale invariants of Floquet topological insulators. *Multiscale Modeling & Simulation*, 20(1):493–523, 2022.
- [8] B. A. Bernevig and T. L. Hughes. *Topological Insulators and Topological Superconductors*. Princeton University Press, 2013.
- [9] J.-M. Bony. *On the Characterization of Pseudodifferential Operators (Old and New)*, pages 21–34. Springer New York, New York, NY, 2013.

[10] Y. Cao, V. Fatemi, S. Fang, K. Watanabe, T. Taniguchi, E. Kaxiras, and P. Jarillo-Herrero. Unconventional superconductivity in magic-angle graphene superlattices. *Nature*, 556(7699):43–50, 2018.

[11] S. Carr, D. Massatt, S. B. Torrisi, P. Cazeaux, M. Luskin, and E. Kaxiras. Relaxation and domain formation in incommensurate 2D heterostructures. *Physical Review B*, page 224102 (7 pp), 2018.

[12] S. Carr, D. Massatt, S. B. Torrisi, P. Cazeaux, M. Luskin, and E. Kaxiras. Relaxation and domain formation in incommensurate two-dimensional heterostructures. *Phys. Rev. B*, 98:224102, Dec 2018.

[13] S. Dai, Y. Xiang, and D. J. Srolovitz. Twisted bilayer graphene: Moiré with a twist. *Nano Letters*, 16(9):5923–5927, 09 2016.

[14] M. Dimassi and J. Sjostrand. *Spectral Asymptotics in the Semi-Classical Limit*. London Mathematical Society Lecture Note Series. Cambridge University Press, 1999.

[15] V. Duchêne and M. I. Weinstein. Scattering, homogenization, and interface effects for oscillatory potentials with strong singularities. *Multiscale Modeling & Simulation*, 9(3):1017–1063, 2011.

[16] P. Elbau and G. Graf. Equality of bulk and edge hall conductance revisited. *Communications in mathematical physics*, 229(3):415–432, 2002.

[17] M. Fruchart and D. Carpentier. An introduction to topological insulators. *Comptes Rendus Physique*, 14(9):779 – 815, 2013. Topological insulators / Isolants topologiques.

[18] C. Gérard and A. Grigis. Precise estimates of tunneling and eigenvalues near a potential barrier. *Journal of differential equations*, 72(1):149–177, 1988.

[19] L. Hörmander. The weyl calculus of pseudo-differential operators. *Communications on Pure and Applied Mathematics*, 32(3):359–443, 1979.

[20] L. Hörmander. *The analysis of linear partial differential operators III: Pseudo-differential operators*. Springer Science & Business Media, 2007.

[21] N. Lerner. *Metrics on the phase space and non-selfadjoint pseudo-differential operators*, volume 3. Springer Science & Business Media, 2011.

[22] E. McCann and M. Koshino. The electronic properties of bilayer graphene. *Reports on Progress in Physics*, 76(5):056503, apr 2013.

[23] E. Prodan and H. Schulz-Baldes. *Bulk and boundary invariants for complex topological insulators*. Springer, Berlin, 2016.

[24] Z. Qiao, J. Jung, Q. Niu, and A. H. MacDonald. Electronic highways in bilayer graphene. *Nano Letters*, 11(8):3453–3459, 08 2011.

[25] S. Quinn and G. Bal. Approximations of interface topological invariants. *arXiv preprint arXiv:2112.02686*, 2021.

[26] P. Rickhaus, J. Wallbank, S. Slizovskiy, R. Pisoni, H. Overweg, Y. Lee, M. Eich, M.-H. Liu, K. Watanabe, T. Taniguchi, T. Ihn, and K. Ensslin. Transport through a network of topological channels in twisted bilayer graphene. *Nano Letters*, 18(11):6725–6730, 11 2018.

[27] P. San-Jose and E. Prada. Helical networks in twisted bilayer graphene under interlayer bias. *Phys. Rev. B*, 88:121408, Sep 2013.

- [28] H. Tang, S. Carr, and E. Kaxiras. Geometric origins of topological insulation in twisted layered semiconductors. *Physical Review B*, 104(15), Oct 2021.
- [29] G. Usaj, P. M. Perez-Piskunow, L. E. F. Foa Torres, and C. A. Balseiro. Irradiated graphene as a tunable floquet topological insulator. *Phys. Rev. B*, 90:115423, Sep 2014.
- [30] F. Zhang, A. H. MacDonald, and E. J. Mele. Valley chern numbers and boundary modes in gapped bilayer graphene. *Proceedings of the National Academy of Sciences*, 110(26):10546–10551, 2013.
- [31] J. Zhou, S. Cheng, W.-L. You, and H. Jiang. Effects of intervalley scattering on the transport properties in one-dimensional valleytronic devices. *Scientific Reports*, 6(1):23211, 2016.

Appendix A: Proof of Theorem 2.1

To begin, we prove the existence of a band gap for all $\lambda \neq 0$:

Firstly, we rescale the system and note we can equivalently show the following system has a gap:

$$H(\xi) = \begin{pmatrix} r + \xi \cdot \sigma & U^* \\ U & -r + \xi \cdot \sigma \end{pmatrix}$$

for $r = \Omega/\lambda$. To understand the effect of the sign of λ and Ω on the topological invariant, we denote $H_{\pm}(\xi, r)$ to include r dependence. Then consider the symmetry operation $\tilde{K} = \sigma_1 \otimes I$. We observe

$$\tilde{K}^{-1} H_{\pm}(\xi, r) \tilde{K} = H_{\mp}(\xi, -r).$$

Hence the sign of r swaps the topology from H_{\pm} to H_{\mp} , and will correspond to a sign swap. To see that a constant symmetry transformation does not change the invariant, see (2.1). However, if $\lambda < 0$ dividing $H_{\pm}(\xi)$ by λ involves swapping the eigenvalues, and thus again swapping the sign of the invariant in (2.1). Therefore if we consider $W_{\pm} := W_{\pm}(\Omega, \lambda)$, we have

$$\begin{aligned} W_{\pm}(-\Omega, \lambda) &= -W_{\pm}(\Omega, \lambda) \\ W_{\pm}(\Omega, -\lambda) &= W_{\pm}(\Omega, \lambda). \end{aligned}$$

For the rest of the proof we assume $r > 0$. Returning to the question of existence of the gap, we claim it is sufficient to show that at no ξ this Hamiltonian has energy 0. To see this, note the eigenvalues are trivially continuous in ξ as the Hamiltonian is continuous in ξ . Further, the eigenvalues go to $\pm\infty$ as $|\xi| \rightarrow \infty$ since the $\xi \cdot \sigma$ block diagonal terms dominate the spectrum for large $|\xi|$, forbidding an accumulation point at 0 energy. Recall the spectrum of $\xi \cdot \sigma$ is $\pm|\xi|$. To show that 0 is not an eigenvalue for any ξ , we consider two steps:

- (a) Show if $|\xi| \neq r$, there is no 0 eigenvalue.
- (b) Show if $|\xi| = r$, there is no 0 eigenvalue.

Part (a): Suppose $\psi = (\psi_1, \psi_2)^T$ is a solution to $H(\xi)\psi = 0$. Then we have the equations

$$(rI + \xi \cdot \sigma)\psi_1 + U^*\psi_2 = 0 \quad \text{and} \quad U\psi_1 + (-rI + \xi \cdot \sigma)\psi_2 = 0.$$

We define

$$R_{\pm} = (\pm rI + \xi \cdot \sigma)^{-1} = g(\xi) \begin{pmatrix} \pm r & \bar{\xi} \\ \xi & \pm r \end{pmatrix}.$$

Here $g(\xi) = \frac{1}{r^2 - |\xi|^2}$ and we denote $\xi = \xi_1 + i\xi_2$ when used as a scalar. Then combining the two equations from the eigenproblem we obtain

$$(I - R_- U R_+ U^*) \psi_2 = 0.$$

A simple calculation shows $U R_+ U^* = r g(\xi) U U^*$. If $U = A$ for example, we obtain

$$I - R_- U R_+ U^* = \begin{pmatrix} 1 + r^2[g(\xi)]^2 & 0 \\ -g(\xi)^2 r \xi & 1 \end{pmatrix}.$$

Since this is invertible, $\psi_2 = 0 \Rightarrow \psi_1 = 0$, and we have no eigenstate corresponding to $E = 0$. Therefore we conclude there is no 0 eigenstate for $|\xi| \neq r$. A symmetric argument holds for $U = A^*$.

Part (b): Suppose $E = 0$ and $|\xi| = r$. Now we denote v_{\pm} to be the eigenstates of $\xi \cdot \sigma$ such that

$$\xi \cdot \sigma v_{\pm} = \pm r v_{\pm}.$$

Assume further that

$$\psi_1 = \alpha_+ v_+ + \alpha_- v_-, \quad \psi_2 = \beta_+ v_+ + \beta_- v_-.$$

We obtain the two equations

$$2r\alpha_+ v_+ + U^* \psi_2 = 0 \quad \text{and} \quad U \psi_1 - 2r\beta_- v_- = 0.$$

We note

$$v_+ = \frac{1}{\sqrt{2}} \begin{pmatrix} 1 \\ \hat{\xi} \end{pmatrix}, \quad v_- = \frac{1}{\sqrt{2}} \begin{pmatrix} 1 \\ -\bar{\xi} \end{pmatrix}. \quad (6.1)$$

Now the image of U^* and U is always a standard basis vector, and thus cannot be proportional to v_{\pm} . Hence by linear independence we have $\alpha_+ = \beta_- = 0$, and $\psi_2 \in \text{Ker}(U^*)$ and $\psi_1 \in \text{Ker}(U)$. These restrictions instantly imply $\psi_1 = \psi_2 = 0$ and we conclude that $H(\xi)$ never has energy 0 for $|\xi| = r$. Combining part (a) and part (b) we see that H has a global gap.

Next we derive the bulk-difference invariant quantity between AB and BA stacking:

Suppose $(\psi_{\pm}^{(j)}, E^{(j)})$ are the eigenpairs ordered from smallest to largest, $j \in \{1, 2, 3, 4\}$. Following [8] Chapter 2, we find we can equivalently replace the expression in (2.1) using

$$T_{\pm}(\xi) = 4\pi i \sum_{i < j} \frac{\text{sign}(E^{(i)}) - \text{sign}(E^{(j)})}{(E^{(i)} - E^{(j)})^2} \Im(\langle \psi_{\pm}^{(i)}, \partial_1 H_{\pm}(\xi) \psi_{\pm}^{(j)} \rangle \langle \psi_{\pm}^{(j)}, \partial_2 H_{\pm}(\xi) \psi_{\pm}^{(i)} \rangle). \quad (6.2)$$

In particular, we have

$$W_{\pm} = \frac{i}{8\pi^2} \int_{\mathbb{R}^2} T_{\pm}(\xi) d\xi. \quad (6.3)$$

Both (6.3) and (2.1) will be used in the proof. We note that η only changes the value of W_{\pm} by a sign, so we neglect it during the proof and simply add the value to the result. We know H_{\pm} have a gap regardless of the parameters Ω, λ . We can rescale our Hamiltonians to write them as

$$H_{\pm}(\xi) = \begin{pmatrix} 1 + \xi \cdot \sigma & \varepsilon U_{\pm}^* \\ \varepsilon U_{\pm} & -1 + \xi \cdot \sigma \end{pmatrix}.$$

Here $U_+ = A$ and $U_- = A^*$. The fundamental idea is to write the invariant as (6.3). We can vary ε at will as this will not close the gap. Therefore we let $\varepsilon \rightarrow 0$, and in the limit we will show the connection $T_{\pm}(\xi)$

localizes around the ring $|\xi| \approx 1$ (see Figure 3). We then find an equivalent gapped 2×2 Hamiltonian over $S^1 \times \mathbb{R}$ with the same invariant, and compute it in this setting.

To build an effective 2×2 system, we project the Hamiltonian onto the eigenstates near energy 0 along the ring. In particular, we consider the 4-vectors

$$v_1 = 2^{-1/2} \begin{pmatrix} v_- \\ 0 \end{pmatrix}, \quad v_2 = 2^{-1/2} \begin{pmatrix} 0 \\ v_+ \end{pmatrix}.$$

We let $Q_{\pm}(\xi) = \{\langle v_i, H_{\pm}(\xi) v_j \rangle\}_{ij}$.

$$Q_+(\xi) = \begin{pmatrix} 1 - |\xi| & \varepsilon \hat{\xi} \\ \varepsilon \hat{\xi} & -1 + |\xi| \end{pmatrix} = (1 - |\xi|) \sigma_3 + \varepsilon \hat{\xi} \cdot \sigma$$

$$Q_-(\xi) = \begin{pmatrix} 1 - |\xi| & -\varepsilon \bar{\hat{\xi}} \\ -\varepsilon \hat{\xi} & -1 + |\xi| \end{pmatrix} = (1 - |\xi|) \sigma_3 - \varepsilon \hat{\xi} \cdot \sigma.$$

We need to show these 2×2 systems admit the same bulk-difference invariant as the 4×4 systems. To do this, we let $V = (v_1, v_2)$. We further let $(q^{\pm}, \pm E)$ be the eigenpairs of $Q_+(\xi)$ (a parallel argument will hold for Q_-). We have

$$H_+ V q^{\pm} \approx \pm E V q^{\pm}.$$

For ε small, we know the Berry curvature is concentrated near the ring $|\xi| \approx 1$ by (6.3). We thus use (2.1) and let $C = \{z \in \mathbb{C} : |z| \in [1/2, 3/2]\}$ (see Figure 3) to obtain:

$$\frac{i}{\pi} \int_C d(V q^+, d(V q^+)) = \frac{i}{\pi} \int_C d(q^+, d q^+) + d(q^+, (V^* dV) q^+).$$

The first term in the limit $\varepsilon \rightarrow 0$ converges to the half-invariant over $S^1 \times \mathbb{R}$. If the second term on the right-hand is zero, then we have the desired relation between the 4×4 invariant and the 2×2 invariant. We can calculate $V^* dV = \hat{\xi} d\bar{\hat{\xi}}$, and thus

$$\int_C d(q^+, (V^* dV) q^+) = \int_{\partial C} \hat{\xi} d\bar{\hat{\xi}} = 0.$$

The final integral is zero as it is an integral over two oppositely oriented circles. Letting $r = |\xi| - 1$ and $e^{i\theta} = \hat{\xi}$ with signs chosen to preserve orientation, we obtain the Hamiltonian

$$H'_{\pm}(\xi) = -r \sigma_3 \pm \varepsilon \cos(\theta) \sigma_1 - \varepsilon \sin(\theta) \sigma_2.$$

We next compute the bulk-difference for this Hamiltonian, which we know from the $\varepsilon \rightarrow 0$ limit correspond to W . We have

$$\partial_r H'_{\pm} = -\sigma_3, \quad \partial_{\theta} H'_{\pm} = \mp \varepsilon \sin(\theta) \sigma_1 - \varepsilon \cos(\theta) \sigma_2.$$

Hence

$$[\partial_r H'_{\pm}, \partial_{\theta} H'_{\pm}] = \pm 2i\varepsilon \sin(\theta) \sigma_2 - 2i\varepsilon \cos(\theta) \sigma_1.$$

We then have

$$\int_0^{2\pi} \text{tr} H'_{\pm} [\partial_r H'_{\pm}, \partial_{\theta} H'_{\pm}] d\theta = \mp 8\pi i \varepsilon^2.$$

Note that $(H'_\pm)^2 = \varepsilon^2 + r^2$. We compute the half invariants

$$W_\pm = \frac{i}{2\pi} \int_{[0,2\pi) \times \mathbb{R}} \frac{-1}{8|H'_\pm|^3} \operatorname{tr} H'_\pm [\partial_r H'_\pm, \partial_\theta H'_\pm] d\theta dr = \pm 1.$$

A derivation of the formula on the left can be found in [2]. Therefore the bulk-difference invariant for this Hamiltonian is $W_- - W_+ = -2$, and generalizing beyond $\eta = 1$ gives bulk-difference invariant -2η .

We then apply Theorem 3.2 in [7] to obtain

$$2\pi\sigma_I = -W = 2\eta.$$

Appendix B: Proof of Theorem 4.1 and relevant notation

We first briefly define the notation used in Section 4 regarding pseudo-differential operators. For a more detailed exposition, see [25, section 2] and references therein.

Given a parameter $h \in (0, 1]$ and a symbol $a(x, \xi; h) \in \mathcal{S}'(\mathbb{R}^d \times \mathbb{R}^d) \otimes \mathbb{M}_n$, we define the Weyl quantization of a as the operator

$$\operatorname{Op}_h(a)\psi(x) := \frac{1}{(2\pi h)^d} \int_{\mathbb{R}^{2d}} e^{i(x-y)\cdot\xi/h} a\left(\frac{x+y}{2}, \xi; h\right) \psi(y) dy d\xi, \quad \psi \in \mathcal{S}(\mathbb{R}^d) \otimes \mathbb{C}^n. \quad (6.4)$$

Here, \mathcal{S} denotes the Schwartz space and \mathbb{M}_n the space of Hermitian $n \times n$ matrices.

A function $u : \mathbb{R}^{2d} \rightarrow [0, \infty)$ is called an order function if there exist constants $C_0 > 0$, $N_0 > 0$ such that $u(X) \leq C_0 \langle X - Y \rangle^{N_0} u(Y)$ for all $X, Y \in \mathbb{R}^{2d}$. Here we use the notation $\langle X \rangle := \sqrt{1 + |X|^2}$. Note that if u_1 and u_2 are order functions, then so is $u_1 u_2$.

We say that $a \in S(u)$ if for every $\alpha \in \mathbb{N}^{2d}$, there exists $C_\alpha > 0$ such that $|\partial^\alpha a(X; h)| \leq C_\alpha u(X)$ for all $X \in \mathbb{R}^{2d}$ and $h \in (0, 1]$. We write $S(u^{-\infty})$ to denote the intersection over $s \in \mathbb{N}$ of $S(u^{-s})$. For $\delta \in [0, 1]$ and $k \in \mathbb{R}$, we say that $a(X; h) \in S_\delta^k(u)$ if for every $\alpha \in \mathbb{N}^{2d}$, there exists $C_\alpha > 0$ such that

$$|\partial^\alpha a(X; h)| \leq C_\alpha u(X) h^{-\delta|\alpha|-k}, \quad (6.5)$$

uniformly in $X \in \mathbb{R}^{2d}$ and $h \in (0, 1]$. If either k or δ are omitted, they are assumed to be zero.

By [14, Chapter 7], we know that if $a \in S(u_1)$ and $b \in S(u_2)$, then $\operatorname{Op}_h(c) := \operatorname{Op}_h(a) \operatorname{Op}_h(b)$ is a pseudo-differential operator, with

$$c(x, \xi) = (a \sharp_h b)(x, \xi) := \left(e^{i \frac{h}{2} (\partial_x \cdot \partial_\xi - \partial_y \cdot \partial_\xi)} a(x, \xi) b(y, \xi) \right) \Big|_{y=x, \xi=\xi}$$

and $c \in S(u_1 u_2)$. We write $A \in \operatorname{Op}_h(S(u))$ to mean that $A = \operatorname{Op}_h(a)$ for some $a \in S(u)$.

Following [9, 19, 21], we define the Hörmander class $S_{1,0}^m$ to be the space of symbols $a(x, \xi)$ that satisfy

$$|(\partial_\xi^\alpha \partial_x^\beta a)(x, \xi)| \leq C_{\alpha, \beta} \langle \xi \rangle^{m-|\alpha|}, \quad \alpha, \beta \in \mathbb{N}^d. \quad (6.6)$$

Given $\phi \in \mathcal{C}_0^\infty(\mathbb{R})$, there exists an almost analytic extension $\tilde{\phi} \in \mathcal{C}_0^\infty(\mathbb{C})$ that satisfies

$$|\bar{\partial} \tilde{\phi}| \leq C_N |\Im z|^N, \quad N \in \{0, 1, 2, \dots\}; \quad \tilde{\phi}(\lambda) = \phi(\lambda), \quad \lambda \in \mathbb{R}. \quad (6.7)$$

We now recall [14, Theorem 8.1]. If H is a self-adjoint operator on a Hilbert space, then

$$\phi(H) = -\frac{1}{\pi} \int \bar{\partial} \tilde{\phi}(z) (z - H)^{-1} d^2 z, \quad (6.8)$$

where $\bar{\partial} := \frac{1}{2} \partial_{\Re z} + \frac{i}{2} \partial_{\Im z}$ and $d^2 z$ is the Lebesgue measure on \mathbb{C} . (6.8) is known as the Helffer-Sjöstrand formula.

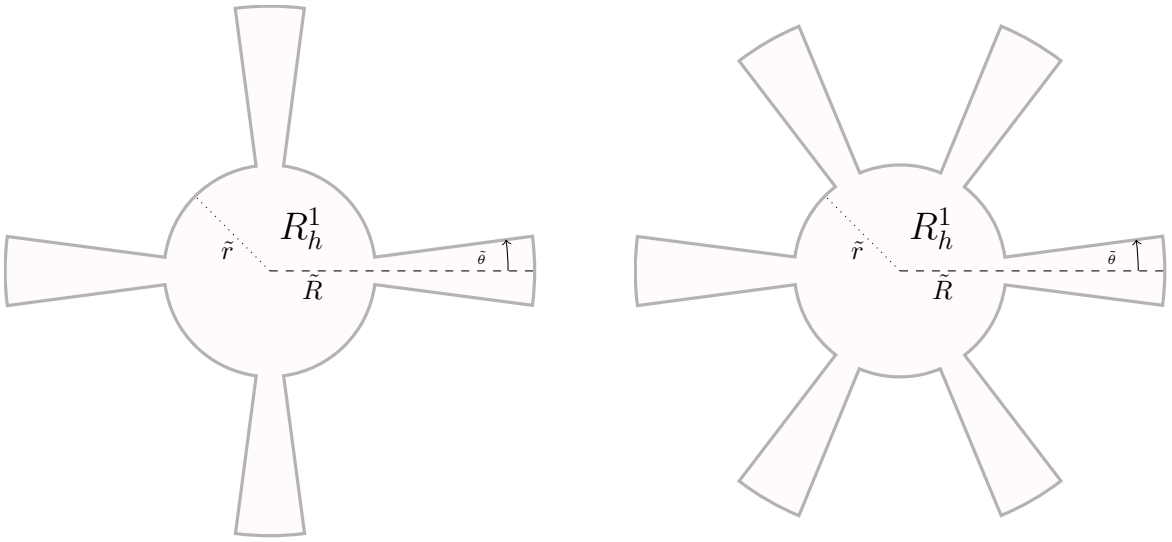


Figure 13: Illustrations of R_h^1 when $k = 2$ (left) and $k = 3$ (right). We integrate over $(x, y) \in R_h^1$ in the proof of Theorem 4.1. Both \tilde{R} and \tilde{r} go to infinity as $h \rightarrow 0$, with the former growing at a faster rate. The angle $\tilde{\theta}$ goes to zero in this limit.

Proof of Theorem 4.1. By assumption, $\varphi' \in \mathcal{C}_c^\infty(E_1 + \eta, E_2 - \eta)$ for some $\eta > 0$. To simplify notation, we redefine $E_1 \leftarrow E_1 + \eta$ and $E_2 \leftarrow E_2 - \eta$. Let p and γ_g be positive constants satisfying $5p + (m + 4)\gamma_g < 1$ and $p - 2\gamma_g > 0$. Let γ_f and γ be positive constants such that $\gamma_f + 2\gamma < \gamma_g < 2\gamma_f$. Let $q < \gamma_g$ be sufficiently large so that $2q - \gamma_f - \gamma_g - 2\gamma > 0$. One could, for example, take

$$(p, \gamma, \gamma_f, q) = (2\gamma_g + \varepsilon, \varepsilon, \gamma_g/2 + \varepsilon, \gamma_g - \varepsilon), \quad \gamma_g = (15 + m)^{-1},$$

for any sufficiently small $\varepsilon > 0$. Define $P_h(x, y) := P(h^q x, h^q y)$. Define $\tilde{R} := h^{-\gamma_g}$, $\tilde{r} := h^{-\gamma_f}$, and $\tilde{\theta} := h^{\gamma_g - \gamma_f}$. Define the “ceiling fan set” (see Figure 13)

$$R_h^1 := \{(r, \theta) : d(\theta, \Theta_k) \leq \tilde{\theta}, r \leq \tilde{R}\} \bigcup \{(r, \theta) : d(\theta, \Theta_k) > \tilde{\theta}, r \leq \tilde{r}\} \subset \mathbb{R}^2,$$

where $d(\theta, \Theta_k) := \min\{|\theta - \phi|_{\mathbb{T}} : \phi \in \Theta_k\}$ and $|\theta - \phi|_{\mathbb{T}} := \min\{|\theta - \phi|, 2\pi - |\theta - \phi|\}$. That is, $d(\theta, \Theta_k)$ is the distance on the torus between the point θ and the (finite) set Θ_k . Define $R_h^2 := [-h^{-\gamma}, h^{-\gamma}]^2$ and $R_h := R_h^1 \times R_h^2 \subset \mathbb{R}^4$. We first prove the following two results.

Lemma 6.1. Define $\text{Op}_h(a_h) := [H_h, P_h]\varphi'(H_h)$ and

$$\sigma_{I, R_h} := \frac{1}{(2\pi h)^2} \text{tr} \int_{R_h} a_h(x, y, \xi, \zeta) dR, \quad dR := dx dy d\xi d\zeta.$$

Then $\sigma_{I, R_h} - \sigma_I \rightarrow 0$ as $h \rightarrow 0$.

Proof. Define $\text{Op}_h(\kappa_h) := [H_h, P_h]$. Then for all $s > 0$, $\kappa_h \in S(\langle h^q g(x, y) \rangle^{-s} \langle \xi, \zeta \rangle^m)$. Proposition 4.2 states that $\varphi'(H_h) \in \text{Op}_h(S(\langle f(x, y), \xi, \zeta \rangle^{-\infty}))$, thus the composition calculus implies that $a_h \in S(\langle f, h^q g, \xi, \zeta \rangle^{-s})$ for all $s > 0$. We know by [14, Theorem 9.4] and Propositions 4.3 and 4.6 that

$$\sigma_I = \frac{1}{(2\pi h)^2} \text{tr} \int_{\mathbb{R}^4} a_h(x, y, \xi, \zeta) dR,$$

hence

$$|\sigma_{I,R_h} - \sigma_I| \leq \frac{1}{(2\pi h)^2} \int_{\mathbb{R}^4 \setminus R_h} |\operatorname{tr} a_h(x, y, \xi, \zeta)| dR \leq \frac{C}{(2\pi h)^2} \int_{\mathbb{R}^4 \setminus R_h} \langle f, h^q g, \xi, \zeta \rangle^{-s} dR.$$

Write $\mathbb{R}^4 \setminus R_h = (R_h^1 \times (\mathbb{R}^2 \setminus R_h^2)) \cup ((\mathbb{R}^2 \setminus R_h^1) \times \mathbb{R}^2) =: S_h \cup T_h$. Since $\operatorname{Vol} R_h^1 \leq Ch^{-\gamma_g - \gamma_f}$ and

$$\int_{S_h} \langle f, h^q g, \xi, \zeta \rangle^{-s} dR \leq C \operatorname{Vol} R_h^1 \int_{\mathbb{R}^2 \setminus R_h^2} \langle \xi, \zeta \rangle^{-s} dR,$$

we can take s sufficiently large such that

$$\frac{1}{(2\pi h)^2} \int_{S_h} \langle f, h^q g, \xi, \zeta \rangle^{-s} dR \longrightarrow 0 \quad \text{as } h \rightarrow 0.$$

We will now prove the same result for the integral over T_h . Observe that

$$\begin{aligned} \frac{1}{(2\pi h)^2} \int_{T_h} \langle f, h^q g, \xi, \zeta \rangle^{-s} dR &\leq \frac{C}{(2\pi h)^2} \int_{\mathbb{R}^2 \setminus R_h^1} \langle f, h^q g \rangle^{-s} dx dy \int_{\mathbb{R}^2} \langle \xi, \zeta \rangle^{-s} d\xi d\zeta \\ &= \frac{C'}{(2\pi h)^2} \int_{\mathbb{R}^2 \setminus R_h^1} \langle f, h^q g \rangle^{-s} dx dy \end{aligned}$$

for all $s > 2$. We see that $\mathbb{R}^2 \setminus R_h^1 = Q_h^1 \sqcup Q_h^2$, where

$$Q_h^1 := \{(r, \theta) : r > \tilde{r}, d(\theta, \Theta_k) > \tilde{\theta}\} \quad \text{and} \quad Q_h^2 := \{(r, \theta) : r > \tilde{R}, d(\theta, \Theta_k) \leq \tilde{\theta}\}.$$

Since $f'_\Theta(\theta) \neq 0$ for all $\theta \in \Theta_k$, there exists $C > 0$ such that $|f(x, y)| = |rf_\Theta(\theta)| \geq Cr\tilde{\theta}$ for all $(x, y) \in Q_h^1$. Thus for any $\eta > 0$ that satisfies $\gamma_g - \gamma_f - (1 - \eta)\gamma_f < 0$, we have

$$|f(x, y)| \geq Cr^\eta r^{1-\eta} \tilde{\theta} \geq Cr^\eta \tilde{r}^{1-\eta} \tilde{\theta} = Cr^\eta h^{-(1-\eta)\gamma_f} h^{\gamma_g - \gamma_f} \geq Cr^\eta$$

uniformly in $(x, y) \in Q_h^1$ and $h \in (0, 1]$. Hence for s sufficiently large (depending on η),

$$\frac{1}{(2\pi h)^2} \int_{Q_h^1} \langle f, h^q g \rangle^{-s} dx dy \leq \frac{C}{(2\pi h)^2} \int_{Q_h^1} r^{-s\eta} dx dy \leq \frac{2\pi C}{(2\pi h)^2} \int_{\tilde{r}}^\infty r^{1-s\eta} dr \longrightarrow 0 \quad \text{as } h \rightarrow 0.$$

Finally we consider the integral over Q_h^2 . Since g_Θ is bounded away from 0 for all θ satisfying $d(\theta, \Theta_k) \leq \tilde{\theta}$ (and h sufficiently small), it follows that

$$\int_{Q_h^2} \langle f, h^q g \rangle^{-s} dx dy \leq \int_{Q_h^2} \langle h^q g \rangle^{-s} dx dy \leq C\tilde{\theta} \int_{\tilde{R}}^\infty (h^q r)^{-s} r dr = \frac{C}{s-2} h^{\gamma_g - \gamma_f} h^{-2\gamma_g} h^{(\gamma_g - q)s}$$

for all $s > 2$. Hence for s sufficiently large, $\frac{1}{(2\pi h)^2} \int_{Q_h^2} \langle f, h^q g \rangle^{-s} dx dy \longrightarrow 0$ as $h \rightarrow 0$. We have thus shown that $\sigma_{I,R_h} - \sigma_I \longrightarrow 0$ as $h \rightarrow 0$, and the proof is complete. \square

Lemma 6.2. Define $z = \lambda + i\omega$ and $\sigma_z = z - \sigma$. There exist $C, h_0 > 0$ such that $|\sigma_z^{-1}| \leq C \langle \xi, \zeta \rangle^{-m} \min\{1, |\omega|^{-1}\}$ uniformly in $(h, \lambda, \omega, x, y, \xi, \zeta) \in (0, h_0] \times [E_1, E_2] \times \mathbb{R} \times (\partial R_h \cap \operatorname{supp}(\nabla P_h))$.

Proof. The arguments from the preceding lemma imply that $\min_{(x,y) \in \partial R_h^1} \langle f(x, y), h^q g(x, y) \rangle \rightarrow \infty$ as $h \rightarrow 0$. By the definition of P_h , it follows that $\min_{(x,y) \in \partial R_h^1 \cap \operatorname{supp}(\nabla P_h)} \langle f(x, y) \rangle \rightarrow \infty$ as $h \rightarrow 0$. Hence for all $(x, y) \in \partial R_h^1 \cap \operatorname{supp}(\nabla P_h)$ and h sufficiently small, $\sigma(x, y, \cdot, \cdot) \in \{\sigma_+(x, y, \cdot, \cdot), \sigma_-(x, y, \cdot, \cdot)\}$. Recalling (H1) and the fact that σ_z is continuous in λ over the compact interval $[E_1, E_2]$, we have thus proved the desired bound uniformly in $(h, \lambda, \omega, x, y, \xi, \zeta) \in (0, h_0] \times [E_1, E_2] \times \mathbb{R} \times (\partial R_h^1 \cap \operatorname{supp}(\nabla P_h)) \times \mathbb{R}^2$. Since $\min_{(\xi,\zeta) \in \partial R_h^2} \langle \xi, \zeta \rangle \rightarrow \infty$ as $h \rightarrow 0$, the desired bound also holds uniformly in $(h, \lambda, \omega, x, y, \xi, \zeta) \in (0, h_0] \times [E_1, E_2] \times \mathbb{R} \times \mathbb{R}^2 \times \partial R_h^2$, and the proof is complete. \square

We now continue the proof of Theorem 4.1. By Proposition 4.6 and Lemma 6.1, it suffices to simplify σ_{I,R_h} . Recalling the composition calculus and the definition of κ_h as the symbol of $[H_h, P_h]$, we find that $\kappa_h \in S_0^{\gamma m-1}(1)$ uniformly in R_h . Indeed, $\sigma \in S_{1,0}^m$ and the definition of R_h imply that

$$|\partial^\alpha \sigma|(x, y, \xi, \zeta) \leq C_\alpha h^{-\gamma m}, \quad (\alpha; h; x, y, \xi, \zeta) \in \mathbb{N}^4 \times (0, 1] \times R_h, \quad (6.9)$$

while the additional factor of h is explained by the vanishing principal symbol of the commutator of two operators whose symbols commute. (Recall also that P_h and all its derivatives are bounded.) Define $\text{Op}_h(\rho_h) := \varphi'(H_h)$. Since $\rho_h \in S(1)$, it follows that

$$\sigma_{I,R_h} = \frac{1}{(2\pi h)^2} \text{tr} \int_{R_h} \kappa_h \sharp_h \rho_h = \frac{1}{(2\pi h)^2} \text{tr} \int_{R_h} (\kappa_h \rho_h + \frac{ih}{2} \{\kappa_h, \rho_h\} + h^2 a_{2,h}) dR,$$

where $\{a, b\} := \partial_x a \partial_\xi b + \partial_y a \partial_\zeta b - \partial_\xi a \partial_x b - \partial_\zeta a \partial_y b$ and $a_{2,h} \in S^{\gamma m-1}(1)$ uniformly in R_h . Using that $\gamma < \gamma_f < \gamma_g$, we have

$$\left| \frac{1}{(2\pi h)^2} \text{tr} \int_{R_h} h^2 a_{2,h} dR \right| \leq C h^{1-\gamma m} \text{Vol } R_h \leq C' h^{1-\gamma_g(m+4)}, \quad (6.10)$$

meaning that

$$\sigma_{I,R_h} = \frac{1}{(2\pi h)^2} \text{tr} \int_{R_h} (\kappa_h \rho_h + \frac{ih}{2} \{\kappa_h, \rho_h\}) dR + o(1)$$

by definition of γ_g .

We will now expand κ_h and ρ_h , and discard noncontributing terms as in (6.10). The composition calculus implies that $\kappa_h = -ih\kappa_{1,h} + \frac{h^2}{4}\kappa_{2,h} + h^3\kappa_{3,h}$, where

$$\kappa_{1,h} = \partial_\xi \sigma_z \partial_x P_h + \partial_\zeta \sigma_z \partial_y P_h, \quad \kappa_{2,h} = \partial_{\xi\xi}^2 \sigma_z \partial_{xx}^2 P_h + 2\partial_{\xi\xi}^2 \sigma_z \partial_{xy}^2 P_h + \partial_{\zeta\zeta}^2 \sigma_z \partial_{yy}^2 P_h,$$

and $\kappa_{3,h} \in S^{\gamma m}(1)$ uniformly in R_h . Define $Z := \{E_1 \leq \lambda \leq E_2\} \times \{|\omega| \leq 2\} \supset \text{supp}(\bar{\partial}\tilde{\varphi}')$ and $Z_\delta := Z \cap \{|\omega| \geq \delta\}$, with $\delta := h^p$. Define $\text{Op}_h(r_{z,h}) := (z - H)^{-1}$. The Helffer-Sjöstrand formula (6.8) implies that

$$\rho_h = -\frac{1}{\pi} \int_{\mathbb{C}} \bar{\partial}\tilde{\varphi}'(z) r_{z,h} d^2 z = -\frac{1}{\pi} \int_Z \bar{\partial}\tilde{\varphi}'(z) r_{z,h} d^2 z,$$

hence

$$\sigma_{I,R_h} = -\frac{1}{\pi} \frac{1}{(2\pi h)^2} \text{tr} \int_{R_h} \int_Z a_{0,h}(x, y, \xi, \zeta) d^2 z dR + o(1), \quad (6.11)$$

where

$$a_{0,h} = \bar{\partial}\tilde{\varphi}'(z) \left((-ih\kappa_{1,h} + \frac{h^2}{4}\kappa_{2,h}) r_{z,h} + \frac{h^2}{2} \{\kappa_{1,h}, r_{z,h}\} \right).$$

Since $a_{0,h}$ involves no derivatives of $r_{z,h}$ that are higher than first order, we can use [14, Proposition 8.6] and the rapid decay of $\bar{\partial}\tilde{\varphi}'$ near the real axis to replace the integral over Z in (6.11) by an integral over Z_δ .

We now expand r_z in terms of σ_z , with all symbolic bounds below uniform in $(x, y, \xi, \zeta, z) \in R_h \times Z_\delta$. Since $\sigma_z \in S^{\gamma m}(1)$ and $r_{z,h} \in S_p^p(1)$ (by (6.9) and [14, Proposition 8.6] respectively), the identity $r_{z,h} \sharp_h \sigma_z = 1$ implies that $r_{z,h} \sigma_z + \frac{ih}{2} \{r_{z,h}, \sigma_z\} + h^2 b_{z,h} = 1$, where $b_{z,h} \in S_p^{3p+\gamma m}(1)$. Thus

$$r_{z,h} = \sigma_z^{-1} - \frac{ih}{2} \{r_{z,h}, \sigma_z\} \sigma_z^{-1} - h^2 b_{z,h} \sigma_z^{-1},$$

with $b_{z,h}\sigma_z^{-1} \in S_p^{4p+\gamma m}(1)$ since $\sigma_z^{-1} \in S_p^p(1)$. Differentiating both sides with respect to $j \in \{x, y, \xi, \zeta\}$, we obtain that

$$\partial_j r_{z,h} = \partial_j \sigma_z^{-1} + h \tilde{c}_{z,h}, \quad r_{z,h} = \sigma_z^{-1} - \frac{ih}{2} \{\sigma_z^{-1}, \sigma_z\} \sigma_z^{-1} + h^2 \tilde{b}_{z,h}, \quad (6.12)$$

with $\tilde{c}_{z,h} \in S_p^{4p+\gamma m}(1)$ and $\tilde{b}_{z,h} \in S_p^{5p+\gamma m}(1)$. It thus follows from familiar arguments (and the assumption $5p + (m+4)\gamma_g < 1$) that

$$\sigma_{I,R_h} = -\frac{1}{\pi} \frac{1}{(2\pi h)^2} \text{tr} \int_{R_h} \int_{Z_\delta} \beta_h(x, y, \xi, \zeta) d^2 z dR + o(1),$$

where

$$\beta_h = \bar{\partial} \tilde{\varphi}'(z) \left((-ih\kappa_{1,h} + \frac{h^2}{4}\kappa_{2,h})(\sigma_z^{-1} - \frac{ih}{2} \{\sigma_z^{-1}, \sigma_z\} \sigma_z^{-1}) + \frac{h^2}{2} \{\kappa_{1,h}, \sigma_z^{-1}\} \right).$$

The term in β_h with a factor of h^3 has vanishing contribution as $h \rightarrow 0$, so we can ignore it. Thus

$$\sigma_I(H_h) = W_{-1,h} + W_{0,h} + o(1),$$

where

$$\begin{aligned} W_{-1,h} &= \frac{i}{4\pi^3 h} \text{tr} \int_{R_h} \int_{Z_\delta} \kappa_{1,h} \sigma_z^{-1} d^2 z dR, \\ W_{0,h} &= -\frac{1}{8\pi^3} \text{tr} \int_{R_h} \int_{Z_\delta} \bar{\partial} \tilde{\varphi}'(z) \left(\frac{1}{2} \kappa_{2,h} \sigma_z^{-1} - \kappa_{1,h} \{\sigma_z^{-1}, \sigma_z\} \sigma_z^{-1} + \{\kappa_{1,h}, \sigma_z^{-1}\} \right) d^2 z dR. \end{aligned} \quad (6.13)$$

We will first simplify $W_{0,h}$. The contribution from the first term in the above integrand vanishes in the semiclassical limit, as

$$\text{tr} \int_{R_h} \int_{Z_\delta} |\bar{\partial} \tilde{\varphi}'(z) \kappa_{2,h} \sigma_z^{-1}| d^2 z dR \leq Ch^{-\gamma_g - \gamma_f - 2\gamma + 2q} \rightarrow 0.$$

Here, we have used that all terms of $\kappa_{2,h}$ contain second order derivatives of P_h and thus $\bar{\partial} \tilde{\varphi}'(z) \kappa_{2,h} \sigma_z^{-1}$ is uniformly bounded by Ch^{2q} over a volume bounded by $Ch^{-\gamma_g - \gamma_f - 2\gamma}$. (Recall that $-\gamma_g - \gamma_f - 2\gamma + 2q > 0$ is the definition of q .) Since σ_z and σ_z^{-1} are analytic in $z \in Z_\delta$, integration by parts yields

$$W_{0,h} = -\frac{i}{16\pi^3} \text{tr} \int_{R_h} \int_{[E_1, E_2]} \tilde{\varphi}'(z) \left(\kappa_{1,h} \{\sigma_z^{-1}, \sigma_z\} \sigma_z^{-1} - \{\kappa_{1,h}, \sigma_z^{-1}\} \right) \Big|_{\omega=-\delta}^{\omega=\delta} d\lambda dR + o(1).$$

The second term above also has vanishing contribution in the $h \rightarrow 0$ limit since it can be written in divergence form. Indeed, applying Fubini's Theorem and the identity $2\{a, b\} = \nabla_{\xi, \zeta} \cdot (a \nabla_{x,y} b - \nabla_{x,y} a b) - \nabla_{x,y} \cdot (a \nabla_{\xi, \zeta} b - \nabla_{\xi, \zeta} a b)$, we integrate by parts to obtain

$$\int_{R_h} \int_{[E_1, E_2]} \tilde{\varphi}'(z) \{\kappa_{1,h}, \sigma_z^{-1}\} \Big|_{\omega=-\delta}^{\omega=\delta} d\lambda dR = \int_{[E_1, E_2]} \int_{\partial R_h} \tilde{\varphi}'(z) \Upsilon(z; x, y, \xi, \zeta) \Big|_{\omega=-\delta}^{\omega=\delta} d\Sigma d\lambda,$$

where $2\Upsilon = (a \partial_y b - \partial_y a b) \nu_\zeta - (a \partial_\zeta b - \partial_\zeta a b) \nu_y + [(y, \zeta) \leftrightarrow (x, \xi)]$ with $a = \kappa_{1,h}$ and $b = \sigma_z^{-1}$. Since Υ vanishes outside $\text{supp}(\nabla P)$ and σ_z^{-1} is well behaved on $\partial R_h \cap \text{supp}(\nabla P)$ (see Lemma 6.2), we have $|\tilde{\varphi}'(z) \Upsilon(z; y, \xi, \zeta)|_{\omega=-\delta}^{\omega=\delta} \leq C\delta$ uniformly in the region of integration. Hence

$$\left| \int_{[E_1, E_2]} \int_{\partial R_h} \tilde{\varphi}'(z) \Upsilon(z; y, \xi, \zeta) \Big|_{\omega=-\delta}^{\omega=\delta} d\Sigma d\lambda \right| \leq C\delta \text{Vol } \partial R_h \leq C\delta h^{-\gamma_g - \gamma_f - \gamma} = Ch^{p - \gamma_g - \gamma_f - \gamma} \rightarrow 0,$$

where we have used the assumption that $p - \gamma_g - \gamma_f - \gamma > p - 2\gamma_g > 0$. We have thus shown that

$$W_{0,h} = -\frac{i}{16\pi^3} \operatorname{tr} \int_{R_h} \int_{[E_1, E_2]} \tilde{\varphi}'(z) \kappa_{1,h} \{\sigma_z^{-1}, \sigma_z\} \sigma_z^{-1} \Big|_{\omega=-\delta}^{\omega=\delta} d\lambda dR + o(1).$$

Without loss of generality (see Proposition 4.3), assume $P \in \mathfrak{S}(0, 1; -1, 0; g(x, y))$. Let $\mathcal{L} := \{x_0(t), y_0(t) : t \in \mathbb{R}\}$ be the range of (x_0, y_0) , with the latter defined in section 4. For simplicity, assume that $\mathcal{L} \subset g^{-1}(0)$. By cyclicity of the trace, we know that

$$\operatorname{tr} \kappa_{1,h} \{\sigma_z^{-1}, \sigma_z\} \sigma_z^{-1} = \operatorname{tr} (\partial_x P_h \partial_\xi \sigma_z \{\sigma_z^{-1}, \sigma_z\}_{y,\zeta} + \partial_y P_h \partial_\zeta \sigma_z \{\sigma_z^{-1}, \sigma_z\}_{x,\xi}) \sigma_z^{-1},$$

where we have defined $\{a, b\}_{\alpha, \beta} := \partial_\alpha a \partial_\beta b - \partial_\beta a \partial_\alpha b$. Integrating by parts, it follows that

$$\begin{aligned} \int_{R_h} \operatorname{tr} \kappa_{1,h} \{\sigma_z^{-1}, \sigma_z\} \sigma_z^{-1} dR &= - \int_{R_h} \operatorname{tr} P_h (\partial_x (\partial_\xi \sigma_z \{\sigma_z^{-1}, \sigma_z\}_{y,\zeta} \sigma_z^{-1}) + \partial_y (\partial_\zeta \sigma_z \{\sigma_z^{-1}, \sigma_z\}_{x,\xi} \sigma_z^{-1})) dR \\ &\quad + \int_{(\mathcal{L} \cap R_h^1) \times R_h^2} \operatorname{tr} (\partial_\xi \sigma_z \{\sigma_z^{-1}, \sigma_z\}_{y,\zeta} \sigma_z^{-1} \nu_x + \partial_\zeta \sigma_z \{\sigma_z^{-1}, \sigma_z\}_{x,\xi} \sigma_z^{-1} \nu_y) d\ell dR_2 + \beta_{z,h}, \end{aligned}$$

where $dR_2 := d\xi d\zeta$ and ℓ is the integration measure on \mathcal{L} , with

$$\int_{[E_1, E_2]} \tilde{\varphi}'(z) \beta_{z,h} \Big|_{\omega=-\delta}^{\omega=\delta} d\lambda \longrightarrow 0 \quad \text{as } h \rightarrow 0. \quad (6.14)$$

Here, ν is the unit vector (outwardly) normal to the surface $\partial(\{-h^{-q} \leq g(x, y) \leq 0\} \cap R_h^1)$. To prove (6.14), we recognized that the integral over R_h is really an integral over $(\{-h^{-q} \leq g(x, y) \leq 0\} \cap R_h^1) \times R_h^2 \supset \operatorname{supp}(\nabla P_h) \times R_h^2$. The boundary term corresponding to $g(x, y) = -h^{-q}$ vanishes since $P_h = 0$ there. The boundary term over $(\{-h^{-q} \leq g(x, y) \leq 0\} \cap \partial R_h^1) \times R_h^2$ has vanishing contribution, as can be verified by applying Lemma 6.2 with the fact that $p > 2\gamma_g > \gamma_g + 2\gamma$. Indeed, the surface area of $(\{-h^{-q} \leq g(x, y) \leq 0\} \cap \partial R_h^1) \times R_h^2$ is bounded by $Ch^{-\gamma_g - 2\gamma}$ with the integrand (including now the evaluation at $\omega = \pm\delta$) bounded by Ch^p .

Again using cyclicity of the trace, we can verify that

$$\operatorname{tr} (\partial_x (\partial_\xi \sigma_z \{\sigma_z^{-1}, \sigma_z\}_{y,\zeta} \sigma_z^{-1}) + \partial_y (\partial_\zeta \sigma_z \{\sigma_z^{-1}, \sigma_z\}_{x,\xi} \sigma_z^{-1})) = 0$$

and

$$-\operatorname{tr} (\partial_\xi \sigma_z \{\sigma_z^{-1}, \sigma_z\}_{y,\zeta} \sigma_z^{-1} \nu_x + \partial_\zeta \sigma_z \{\sigma_z^{-1}, \sigma_z\}_{x,\xi} \sigma_z^{-1} \nu_y) = \operatorname{tr} (\nu_x \partial_y \sigma_z - \nu_y \partial_x \sigma_z) \{\sigma_z^{-1}, \sigma_z\}_{\xi,\zeta} \sigma_z^{-1}.$$

We recognize the first factor on the above right-hand side as the derivative of σ_z in the direction of \mathcal{L} (with t increasing). We conclude that

$$W_{0,h} = \frac{i}{16\pi^3} \operatorname{tr} \int_{T_h} \int_{[E_1, E_2]} \tilde{\varphi}'(z) \partial_t \tau_z \{\tau_z^{-1}, \tau_z\}_{\xi,\zeta} \tau_z^{-1} \Big|_{\omega=-\delta}^{\omega=\delta} d\lambda dR_3 + o(1), \quad (6.15)$$

where $T_h := [-t_h, t_h] \times R_h^2 \subset \mathbb{R}^3$ with $t_h := \sup\{|t| : (x_0(t), y_0(t)) \in R_h^1\} < \infty$, and $dR_3 := dt d\xi d\zeta$. Here, we have used that $\partial_t \tau = x'_0(t) \partial_x \sigma + y'_0(t) \partial_y \sigma = N(\nu_y \partial_x \sigma - \nu_x \partial_y \sigma)$ and $d\ell = N dt$, with $N := \sqrt{(x'_0(t))^2 + (y'_0(t))^2}$.

We next eliminate $\tilde{\varphi}'(z)$ from (6.15). Since $\partial_t \tau_z \{\tau_z^{-1}, \tau_z\}_{\xi,\zeta} \tau_z^{-1} \rightarrow 0$ as $|\omega| \rightarrow \infty$, we have

$$\partial_t \tau_z \{\tau_z^{-1}, \tau_z\}_{\xi,\zeta} \tau_z^{-1} \Big|_{\omega=\pm\delta} = \int_{\pm\infty}^{\pm\delta} \partial_\omega (\partial_t \tau_z \{\tau_z^{-1}, \tau_z\}_{\xi,\zeta} \tau_z^{-1}) d\omega.$$

Cyclicity of the trace and the fact that $\partial_\omega \tau_z = i$ imply that

$$\mathrm{tr} \partial_\omega (\partial_t \tau_z \{ \tau_z^{-1}, \tau_z \}_{\xi, \zeta} \tau_z^{-1}) = i \mathrm{tr} \varepsilon_{ijk} \partial_k (\tau_z^{-1} \partial_i \tau_z \tau_z^{-1} \partial_j \tau_z \tau_z^{-1}), \quad (6.16)$$

where ε_{ijk} is the anti-symmetric tensor with $\varepsilon_{123} = 1$, and the variables are identified by $(1, 2, 3) = (\xi, \zeta, t)$. Pulling ∂_k out of the integral over ω and integrating by parts, we get

$$\mathrm{tr} \int_{T_h} \partial_t \tau_z \{ \tau_z^{-1}, \tau_z \}_{\xi, \zeta} \tau_z^{-1} \Big|_{\omega=\pm\delta} dR_3 = i \int_{\partial T_h} \int_{\pm\infty}^{\pm\delta} \Theta d\omega d\Sigma, \quad \Theta := \mathrm{tr} \varepsilon_{ijk} \tau_z^{-1} \partial_i \tau_z \tau_z^{-1} \partial_j \tau_z \tau_z^{-1} \nu_k,$$

where ν is the outward unit normal vector to the surface ∂T_h , and Σ is the Euclidean surface measure in \mathbb{R}^3 . Since $\tilde{\varphi}'$ is smooth, (h1) implies that

$$W_{0,h} = -\frac{1}{16\pi^3} \int_{[E_1, E_2]} \varphi'(\lambda) \int_{\partial T_h} \int_{|\omega| \geq \delta} \Theta d\omega d\Sigma d\lambda + o(1).$$

Integrating by parts in λ , we obtain

$$W_{0,h} = -\frac{1}{16\pi^3} \int_{\partial T_h} \int_{|\omega| \geq \delta} \Theta d\omega d\Sigma + o(1),$$

with now $z = E_2 + i\omega$ in the above integrand (and from now on). The fact that only the boundary term survives follows from analyticity of Θ in z over the region of integration (so that $\partial_\lambda \Theta = -i\partial_\omega \Theta$) and by now familiar arguments. Applying (6.16) in reverse, we conclude that

$$W_{0,h} = \frac{i}{16\pi^3} \int_{T_h} \mathrm{tr} \partial_t \tau_z \{ \tau_z^{-1}, \tau_z \}_{\xi, \zeta} \tau_z^{-1} \Big|_{\omega=-\delta}^{\omega=\delta} dR_3 + o(1).$$

We now recognize that $\{\omega = \pm\delta\} \times T_h \subset \partial T_h^4$, where $T_h^4 := [-\delta, \delta] \times T_h$. Observe that for all (i, j, k, ℓ) permutations of (ω, ξ, ζ, t) , the integral of $\mathrm{tr} \partial_i \tau_z \tau_z^{-1} \partial_j \tau_z \tau_z^{-1} \partial_k \tau_z \tau_z^{-1} \nu_\ell$ over the rest of ∂T_h^4 vanishes in the semiclassical limit, as $\partial T_h^4 \setminus (\{\omega = \pm\delta\} \times T_h) \subset \mathbb{R} \times \partial T_h$. By cyclicity of the trace, it follows that

$$W_{0,h} = \frac{i}{48\pi^3} \int_{\partial T_h^4} u \cdot \nu d\Sigma + o(1), \quad u_\ell = \mathrm{tr} \varepsilon_{ijk\ell} \partial_i \tau_z \tau_z^{-1} \partial_j \tau_z \tau_z^{-1} \partial_k \tau_z \tau_z^{-1},$$

with Σ now the Euclidean surface measure in \mathbb{R}^4 , the variables $(1, 2, 3, 4) = (\omega, \xi, \zeta, t)$ and $\varepsilon_{ijk\ell}$ the anti-symmetric tensor with $\varepsilon_{1234} = 1$. A direct computation reveals that $\nabla \cdot u = 0$ in $(T_h^4 \setminus R) \cup (R \setminus T_h^4)$, hence $W_{0,h} = \frac{i}{48\pi^3} \int_{\partial R} u \cdot \nu d\Sigma + o(1)$ by the Divergence Theorem.

We have thus shown that

$$\sigma_I(H_h) - \frac{i}{48\pi^3} \int_{\partial R} u \cdot \nu d\Sigma = W_{-1,h} + o(1),$$

with $W_{-1,h}$ given by (6.13). By Proposition 4.6, the left-hand side is independent of $h \in (0, 1]$ and the parameters $(p, \gamma_g, \gamma_f, \gamma)$ satisfying the constraints in the first paragraph of this proof. From the h -independence, we know there exists $c \in \mathbb{C}$ such that $W_{-1,h} \rightarrow c$ as $h \rightarrow 0$. To show that in fact $c = 0$, consider the semiclassical limit of $W_{-1,h}$ under two different choices for the parameters, say $(p, \gamma_g, \gamma_f, \gamma) = (\frac{1}{12}, \frac{1}{96(m+4)}, \frac{1}{180(m+4)}, \frac{1}{720(m+4)})$ and $(p', \gamma'_g, \gamma'_f, \gamma') = \frac{1}{2}(p, \gamma_g, \gamma_f, \gamma)$. Then $R_h = R'_{h^2}$ and $\delta(h) = \delta'(h^2)$, so that $h^{1/2} W_{-1,h} \rightarrow c$ as $h \rightarrow 0$.

We conclude that

$$\sigma_I(H) = \frac{i}{48\pi^3} \int_{\partial R} u \cdot \nu d\Sigma, \quad (6.17)$$

with $\Re(z) = E_2$ in the above integrand. Since the right-hand side is independent of $\varphi \in \mathfrak{S}(0, 1; E_1, E_2)$, we apply (6.17) with $\varphi \in \mathfrak{S}(0, 1; E_1, \alpha)$ to complete the result. \square